

## EXPANSION JOINTS IN HYPERBOLIC MANIFOLDS

ALEX ELZENAAR

ABSTRACT. Deformations of hyperbolic manifolds through metrics with cone singularities along closed loops were first studied by Thurston as continuous realisations of Dehn fillings. Instead of gluing singular solid tori into rank 2 cusps, we glue singular 2-handles into rank 1 cusps. Our method is to find substructures within which the hyperbolic metric can be ‘fractured’ in a controlled way by direct manipulation of a fundamental polyhedron, changing the cone angle around an ideal arc to interpolate between cusped hyperbolic manifolds and hyperbolic manifolds with conformal surfaces on the visual boundary. As an application, we use cone deformations of a family of arithmetic manifolds derived from the Borromean rings to show that the upper unknotting tunnels of highly twisted 2-bridge links can be drilled out by cone deformations. We also show that our structures arise naturally in fully augmented links, providing a large family of examples.

## 1. INTRODUCTION

Hyperbolic cone manifolds (see [6, §3] for definitions) provide geometric structures which interpolate between complete hyperbolic metrics on different topological manifolds: hyperbolic cusps are limiting cases of cone singularities where the cone angle is 0, and arcs away from the singular locus are limiting cases where the cone angle is  $2\pi$ . The holonomy group of a hyperbolic cone manifold is a subgroup of  $\mathrm{PSL}(2, \mathbb{C})$  but is only discrete if the cone angles are submultiples of  $2\pi$  (i.e. the cone manifold is an orbifold). It was observed by Thurston [43, §4.4–4.5] (see also [42]) that a path of cone manifolds in which a cone angle around a closed loop is increased from 0 to  $2\pi$  is a continuous realisation of a Dehn filling, with slope depending on the choice of holonomy element which becomes elliptic. This idea was been used by Brock and Bromberg [8; 9] to prove a version of the density conjecture for Kleinian groups, and by Hodgson and Kerchoff [25] and Futer, Purcell, and Schleimer [19; 20] to compare the hyperbolic metric on a link complement to that on its Dehn fillings by showing that the metric on a family of interpolating cone manifolds is controlled.

We wish to study the geometry of finite volume hyperbolic 3-manifolds like link complements by cone-deforming them into manifolds with nontrivial conformal boundary in a controlled way. This is motivated by questions about geodesicity of certain embedded arcs in link complements (we provide a straightforward application of this type as [Theorem 3.7](#)) and by a more general need for effective tools that can compare finite and infinite covolume Kleinian groups. To model the topological operation of gluing in a 2-handle across a rank 1 cusp with a path of cone manifolds,

---

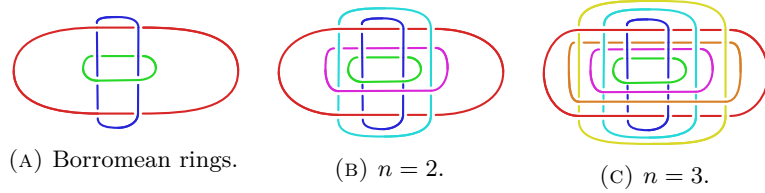
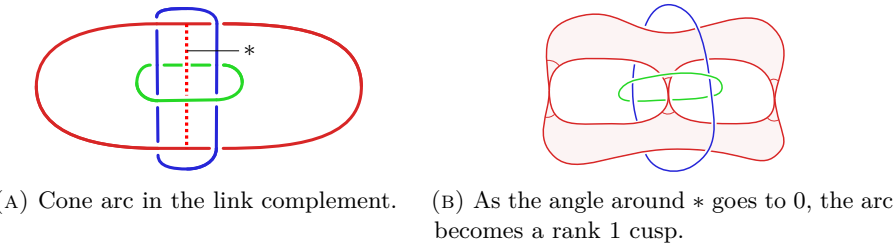
SCHOOL OF MATHEMATICS, MONASH UNIVERSITY, MELBOURNE

*E-mail address:* [alexander.elzenaar@monash.edu](mailto:alexander.elzenaar@monash.edu).

*2020 Mathematics Subject Classification.* Primary 57K35; Secondary 20H10, 52B70, 57K10, 57K32, 57M50, 58H15.

*Key words and phrases.* Kleinian groups, cone manifolds, two-bridge links, unknotting tunnels, Borromean rings, ideal octahedra, Poincaré polyhedron theorem, fully augmented links, geometrically isolated cusps, deformations of hyperbolic structures.

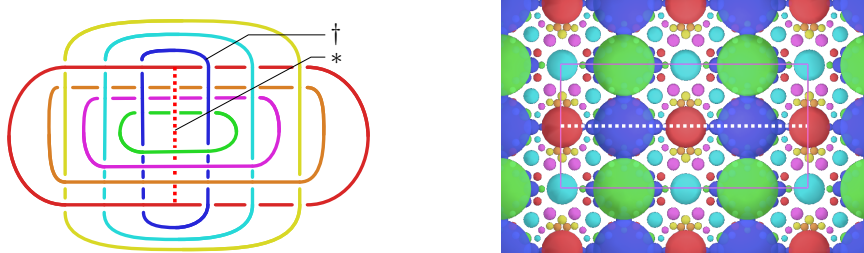
The author was supported by an Australian Government Research Training Program (RTP) Scholarship during the period that this work was undertaken.

FIGURE 1. The  $n$ -stacked Borromean rings for small  $n$ .FIGURE 2. The lantern manifold is produced by deforming the cone angle in the Borromean rings complement around the dotted arc  $*$  from  $2\pi$  to 0.

we need to be able to deform cone angles around an ideal arc continuously through the interval  $[0, 2\pi]$ . An abstract framework to prove existence of cone deformations was a major programme of work in the early 21st century building on ideas of Hodgson and Kerckhoff [24], see also Weiß [44; 45] and Kojima [28] for the case that the singular locus is a link and Weiß [46] and Montcouquiol [32] for the case that the singular locus is a graph. Unfortunately, to apply the global results of this theory in practice it is necessary to obtain detailed technical estimates such as injectivity radius bounds. One of the major difficulties is that there may be some ‘critical angle’ where the metric ceases to be hyperbolic (see e.g. [13; 22; 23; 38; 39]). Thus to work with specific examples it is often still necessary to construct the deformations explicitly by hand [4; 15; 48].

In this paper, we exhibit and study substructures in hyperbolic 3-manifolds which isolate a family of rank 2 cusps and allow arcs joining them to be cone-deformed to form new rank 1 cusps. In the process the metric around the cusps is fractured so that they bubble into punctured surfaces on the conformal boundary, while the remainder of the manifold remains geometrically controlled. We call these structures *expansion joints* since they behave like expansion joints on a bridge, allowing two halves of the manifold to move apart and isolating all stress in a single location. Other geometric isolation phenomena were observed by Neumann and Reid [33; 34], see also the later work of Kapovich [27] and Calegari [10; 11]; they gave examples of 3-manifolds in which some cusps can be filled via a cone deformation while preserving the Euclidean structure on other cusps. After doubling across the conformal boundary, our form of isolation is similar except that there is a rank 2 cusp which is transverse to the region containing cone deformations. Another approach to the study of cusp shape changes upon cone deformations is due to Purcell [41], who used the Hodgson–Kerckhoff theory to bound changes to the Euclidean metrics on cusp tori; our method gives stronger results when it applies, but requires control over a local polyhedral decomposition.

Our starting point is a family of arithmetic links called *stacked Borromean rings* (Definition 3.1) obtained by choosing a distinguished ‘central’ component of the



(A) The manifold  $M^n$  is produced from  $B^n$  by decreasing the cone angle around the dotted arc  $*$  from  $2\pi$  to 0.

(B) Cusp horoballs for  $B^3$ , with  $\dagger$  at  $\infty$ . The geodesic arc  $*$  lifts to a family of geodesic arcs above the dotted horizontal line.

FIGURE 3. The combinatorics and geometry of  $B^3$ .

Borromean rings and repeating the other two components radially outwards  $n$  times as shown in Figure 1 to obtain  $2n + 1$  loops in total. The complement in  $\mathbb{S}^3$  of the  $n$ -stacked Borromean rings, denoted  $B^n$ , admits a complete hyperbolic structure. For  $n = 1$  (the usual Borromean rings) this is classical: a geometric proof may be found in Thurston [43, §3.4], and an algebraic proof following Riley may be found in Wielenberg [47]. For  $n > 1$  this will be proved as Theorem 3.2. In Proposition 2.4, we prove that there is a continuous path of hyperbolic cone manifolds which interpolate between the Borromean rings complement and the *lantern manifold* shown in Figure 2(B) (the name is chosen since the motivation for its study came from the lantern configuration in mapping class theory [17, §5.1.1]). The cone metrics on the path each have a single singular arc, labelled with  $*$  in Figure 2(A), with cone angle ranging from  $2\pi$  to 0. Our first main result is a generalisation of this cone deformation to all stacked Borromean rings:

**Main Theorem A** (Theorem 3.5). *There exists a smooth path  $p : [0, 2\pi] \rightarrow \text{Hom}(F_{2n+2}, \text{PSL}(2, \mathbb{C}))$  so that for each  $\theta > 0$  the image  $p(\theta)$  is the holonomy group of a hyperbolic cone manifold, supported on  $B^n$ , with a single singular arc indicated in Figure 3(A) of angle  $\theta$ . When  $\theta = 0$ ,  $p(\theta)$  is the holonomy group of the complete hyperbolic manifold obtained by drilling the singular arc from  $B^n$ .*

One indication that the manifolds  $B^n$  should admit a nice theory for their hyperbolic structure comes from plotting horoball neighbourhoods of their cusps as shown for  $n = 3$  in Figure 3(B). Our horoball images were produced by SnapPy [14], and for detailed information on how to interpret these figures see Thurston [42]. An important theme in this paper is that the expansion joint cone-deformations which we construct arise from structures that can be guessed from these figures.

Main Theorem A is proved by first using the symmetries visible in the cusp diagram to decompose  $B^n$  into ideal right-angled octahedra and then deforming the induced fundamental polyhedron in  $\mathbb{H}^3$ . Decompositions of knot and link complements into right-angled octahedra are of independent interest in knot theory, due to their connections with number theory and the geometry of circle packings, see e.g. [26; 37; 40]. As an application of Main Theorem A, we prove in Theorem 3.7 that the upper unknotting tunnel of a highly twisted two-bridge knot can be cone-deformed from angle  $2\pi$  to angle 0; it is this application which originally motivated the definition of stacked Borromean rings.

The specific example of  $B^n$  is just a convenient setting for describing our methods that is complex enough to show most of the interesting features, and in the final section of the paper we describe a more general kind of expansion joint:

**Main Theorem B (Theorem 4.2).** *There exists a polyhedral substructure  $\mathcal{L}$ , which can be detected locally in a hyperbolic 3-manifold and which deformation-retracts onto an embedded geodesic surface, that acts as an expansion joint. That is, its existence in a manifold  $M$  allows the construction of a smooth path of cone manifold structures on  $M$  that, in the limit, deforms a family of rank 2 cusps into a family of embedded thrice-punctured spheres, without modifying the hyperbolic structure of  $M$  away from  $\mathcal{L}$ .*

As an application of Main Theorem B, we show in Theorem 4.5 that all holonomy groups of fully augmented link complements can be obtained by taking an infinite covolume Kleinian group and continuously deforming a parabolic element through infinite order elliptics until it becomes the identity in such a way that all intermediate groups are holonomy groups of cone manifolds with no unexpected singularities. This exhibits every fully augmented link group as the starting point of a smooth arc embedded inside some character variety, parameterising controlled indiscrete groups, that ends on the boundary of a nontrivial quasiconformal deformation space.

In order for the paper to be self-contained we include, in Appendix A, a version of the Poincaré polyhedron theorem for cone manifolds which is well-known but to the best of our knowledge does not appear explicitly in the literature. We also indicate how to write down Maskit combination theorems for cone manifold holonomy groups. This is an important tool in our general programme to apply the theory of Kleinian groups to well-behaved indiscrete subgroups of  $\text{PSL}(2, \mathbb{C})$  in order to join different islands of discreteness in the character variety.

*Convention.* All polyhedra are metric polyhedra (i.e. are locally modelled by intersections of half-spaces). Any exceptions will be called *combinatorial polyhedra*.

**Acknowledgments.** I thank Jessica Purcell for discussion surrounding this work. Many images of knot diagrams and cusp horoballs were produced by the `SnapPy` software [14].

## 2. THE CLASSICAL BORROMEEAN RINGS

We consider the topological 3-manifold  $M$  obtained by drilling two closed loops from a genus 2 handlebody as in Figure 4. The group  $\pi_1(M)$  is generated by the four loops  $A, X, Y, Z$  shown in the figure. The manifold  $M$  has a complete hyperbolic structure if and only if there exists a faithful discrete representation  $\rho : \pi_1(M) \rightarrow \text{PSL}(2, \mathbb{C})$  such that  $M \simeq_{\text{homeo}} \mathbb{H}^3 / \rho(\pi_1(M))$ . We will construct such a representation, with the additional condition that the loops  $Y, Z$ , and  $ZY^{-1}$  are homotopic to rank 1 cusps on the conformal boundary of  $M$ , as in Figure 2(B); this forces  $\rho$  to be a maximal cusp representation on the boundary of the quasiconformal deformation space of all hyperbolic structures, and in particular it will be rigid. Identifying the four generators of  $\pi_1(M)$  with their images in  $\text{PSL}(2, \mathbb{C})$ , the representation must satisfy the conditions in Table 1. These conditions come from the usual relator for a genus 2 surface group, together with commutation conditions for the torus boundary components; we write  $[R, S]$  for the commutator  $RSR^{-1}S^{-1}$ . It is not clear *a priori* that these relations are sufficient to pin down the hyperbolic structure, but we will show in Proposition 2.1 that they are.

We will convert these conditions into a set of polynomial equations in  $\text{GL}(2, \mathbb{C}[\vec{x}])$  where  $\vec{x}$  is some suitable list of indeterminates. Up to conjugacy, we may take

$$A = \begin{bmatrix} 1 & 1 \\ 0 & 1 \end{bmatrix} \quad \text{and} \quad X = \begin{bmatrix} 1 & 0 \\ a_3 & 1 \end{bmatrix}.$$

This takes care of  $\text{tr}^2 A = 4$  and  $\text{tr}^2 X = 4$ . (It is not *a priori* clear that we should be able to choose a global lift from  $\text{PSL}$  to  $\text{SL}$  where  $\text{tr} A$  and  $\text{tr} X$  have equal sign,

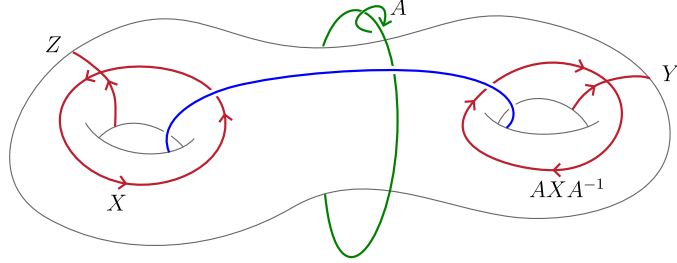


FIGURE 4. The lantern manifold  $M$ : a genus 2 handlebody with two drilled loops. Here, and elsewhere in the paper, manifolds are drawn from the perspective of a viewer in the interior.

TABLE 1. Equations cutting out the character variety.

Surface:	
Rank 1 cusps	$\text{tr}^2 Z = \text{tr}^2 Y = \text{tr}^2 ZY^{-1} = 4$
Surface relation	$[Z^{-1}, X][Y^{-1}, AXA^{-1}]^{-1} = \text{Id}$
Vertical rank 2 cusp:	
Meridian	$\text{tr}^2 A = 4$
Longitude	$\text{tr}^2 [Z^{-1}, X] = 4$
Abelian	$[A, [Z^{-1}, X]] = \text{Id}$
Horizontal rank 2 cusp:	
Meridian	$\text{tr}^2 X = 4$
Longitude	$\text{tr}^2 ZA^{-1}Y^{-1}A = 4$
Abelian	$[X, ZA^{-1}Y^{-1}A] = \text{Id}$

but the assumption is justified *a posteriori* as it leads to a solution.) We now let

$$Y = \begin{bmatrix} b_1 & b_2 \\ b_3 & b_4 \end{bmatrix} \quad \text{and} \quad Z = \begin{bmatrix} c_1 & c_2 \\ c_3 & c_4 \end{bmatrix}$$

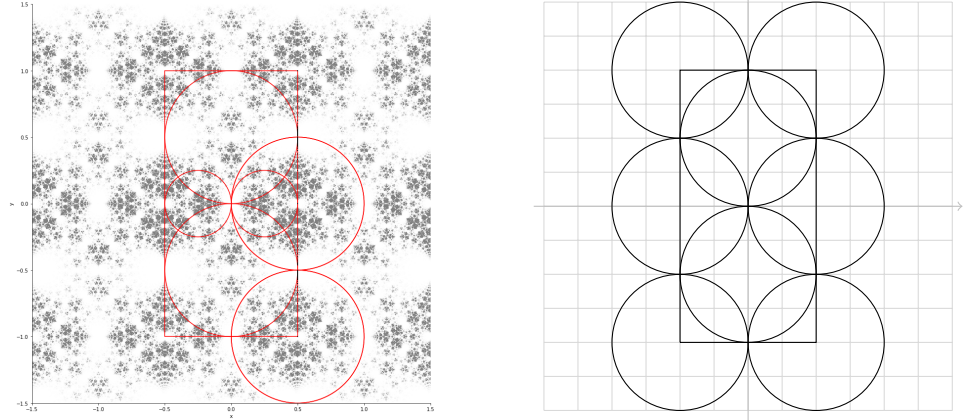
where the  $b_i$  and  $c_i$  are complex indeterminates. We impose on these the determinant conditions  $\det Y = \det Z = 1$ , the remaining trace conditions in the table, and the surface relation  $[Z^{-1}, X] = \pm[Y^{-1}, AXA^{-1}]$ . Since we chose  $A$  and  $X$  to have fixed points at  $\infty$  and 0 respectively and parabolics commute if and only if they share fixed points,  $[A, [Z^{-1}, X]] = \text{Id}$  if and only if  $[Z^{-1}, X]_{(2,1)} = 0$  (here, the subscript denotes matrix indexing; i.e. we are requiring the lower-left entry of the matrix  $[Z^{-1}, X]$  to be 0) and  $[X, ZA^{-1}Y^{-1}A] = \text{Id}$  if and only if  $(ZA^{-1}Y^{-1}A)_{(1,2)} = 0$ . All together we obtain an *a priori* overdetermined polynomial system, which has a 0-dimensional solution set:

**Proposition 2.1.** *There are exactly 16 solutions in  $\mathbb{C}^9$  to the polynomial system just described which satisfy the non-degeneracy conditions*

$$a_3 \neq 0, \quad [Z^{-1}, X]_{(1,2)} \neq 0, \quad \text{and} \quad (ZA^{-1}Y^{-1}A)_{(2,1)} \neq 0,$$

which prevent various parabolics from degenerating to the identity. Eight of these give groups conjugate after change of generators to the group  $G_{2\pi}$  with parameters

$$(a_3, b_1, b_2, b_3, b_4, c_1, c_2, c_3, c_4) = (-2i, -i, 1, -2i, 2+i, i, -1, 2i, -2-i).$$



(A) Limit set and isometric circles of  $X$  and  $Z A^{-1} Y^{-1} A$  (the respective meridian and longitude of the cusp descending from 0), and  $Y = Z$  (the meridian of the cusp coloured red in Figure 1(A)).

(B) The solid circles and lines give the projection of a fundamental domain onto the Riemann sphere. Grid squares have width 0.25.

FIGURE 5. Data associated with the Borromean rings group  $G_{2\pi}$ .

TABLE 2. Side-pairing transformations for Figure 6(B).

$1 \leftrightarrow 2$	$X$		
$3 \leftrightarrow 5$	$Z$	$4 \leftrightarrow 6$	$A^{-1}YA$
$7 \leftrightarrow 3$	$XZX^{-1}$	$8 \leftrightarrow 4$	$XA^{-1}YAX^{-1}$
Translations: $A$ (horiz.), $Z^{-1}XZX^{-1}$ (vert.)			

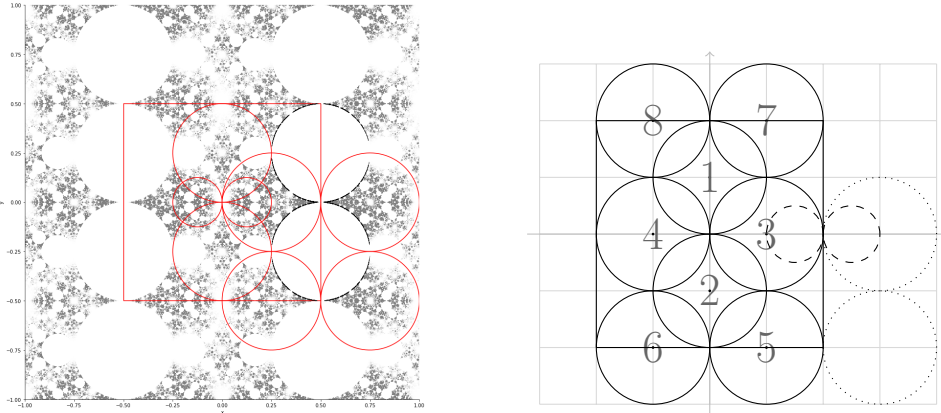
The remaining eight give groups conjugate after change of generators to the group  $G_0$  with parameters

$$(a_3, b_1, b_2, b_3, b_4, c_1, c_2, c_3, c_4) = \left( -4i, -3i, \frac{3}{2} + 2i, -4i, 2 + 3i, i, -\frac{1}{2}, 4i, -2 - i \right).$$

*Proof.* The system of equations may be solved exactly by computer algebra systems (e.g. using the `Reduce` command in `Mathematica`) to verify that there are 16 solutions; the conjugacies that can be defined to separate these into the two sets of 8 are essentially immediate from the symmetries of the solutions.  $\square$

**Example 2.2** (The Borromean rings). The group  $G_{2\pi}$  admits the relation  $ZY^{-1} = \text{Id}$ . In fact it is essentially the same realisation of the Borromean rings group as that constructed by Wielenberg [47, Example 8]. We show the limit set and fundamental domain in Figure 5, which should be compared with Figure 12 *op. cit.*

**Example 2.3** (The lantern group). We claim that  $G_0$  is the holonomy group of a complete hyperbolic structure on the manifold  $M$ . Plotting the limit set and isometric circles of the various words that appear in Table 1 we obtain Figure 6(A), which suggests the construction of the fundamental domain given in Figure 6(B) (the four corners of the square are at  $\pm\frac{1}{2} \pm \frac{1}{2}i$  and all circles that appear orthogonal or tangent are so). The side-pairings are given in Table 2. From Figure 6(B) it is possible to immediately read off an ideal triangulation for the convex core of  $M$ .



(A) Limit set and isometric circles of  $X$  and  $ZA^{-1}Y^{-1}A$  (the respective meridian and longitude of the cusp descending from 0), and  $Y$  and  $Z$  (which generate the stabiliser of one of the thrice-punctured sphere components).

(B) The solid circles and lines give the projection of a fundamental domain onto the Riemann sphere. The two dotted circles are paired by  $Y$ , and the two dashed circles are paired by  $ZY^{-1}$ . Grid squares have width 0.25.

FIGURE 6. Data associated with the lantern group  $G_0$ .

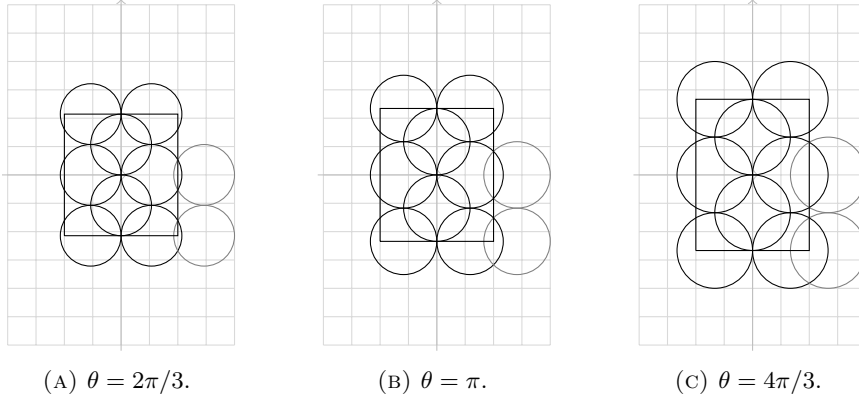


FIGURE 7. Cone-deforming the Borromean rings to the lantern manifold. Each figure shows the fundamental domain for some  $G_\theta$ .

**Proposition 2.4.** *There exists a smooth family of cone manifold holonomy groups  $G_\theta$  interpolating between  $G_0$  and  $G_{2\pi}$ ; the manifold uniformised by  $G_\theta$  for  $\theta \in (0, 2\pi]$  is supported on the complement of the Borromean rings, and has an ideal singular arc with cone angle  $\theta$  along the arc labelled  $*$  in Figure 2(A); as  $\theta \rightarrow 0$ , the manifolds limit onto the lantern manifold and  $G_\theta \rightarrow G_0$ .*

*Proof.* The deformation is defined by continuously moving the walls of the fundamental domain while preserving its combinatorics and geometry away from the faces paired by  $ZY^{-1}$ . From a comparison of Figure 6(B) with Figure 5(B), a naïve description of the deformation is that we smoothly change the aspect ratio of the rank two lattice fixing  $\infty$  from  $1:2$  to  $1:1$ , as in Figure 7.

To give a formal definition of the polyhedra used to define  $G_\theta$ , observe that as the circles paired by  $Y$  and the circles paired by  $Z$  begin to overlap as the aspect ratio of the rectangle is changed, the angle between them is twice the angle between the

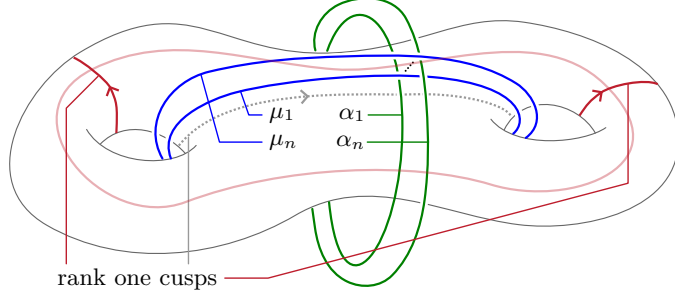


FIGURE 8. The  $n$ -stacked lantern manifold  $M^n$ . The central cusp  $\chi$  has become a closed loop on the genus 2 surface, dual to two rank 1 cusps.

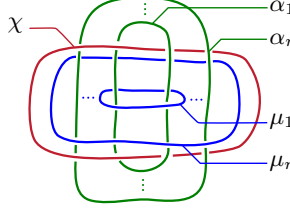
two isometric circles of  $ZY^{-1}$ . Thus, for the full deformation, as the angle between the two isometric circles of  $ZY^{-1}$  is deformed from 0 (at  $G_0$ ) to  $2\pi$  (at  $G_{2\pi}$ ), the angle between the isometric circle of  $Z$  and the isometric circle of  $Y$  deforms from 0 to  $\pi$ . Since we have normalised  $A$  to be the translation  $z \mapsto z + 1$ , the width of the rectangle is fixed and so the height must vary to change the aspect ratio. The radius of the isometric circles of  $Y$  and  $Z$  is  $1/4$  of the height of this rectangle, and an elementary trigonometric calculation shows that if the angle between the isometric circle of  $Y$  and the isometric circle of  $Z$  is  $2\theta$ , then the radii of those circles is  $r_\theta = \frac{1}{4} \sec^2 \frac{\theta}{2}$ .

This quantity is enough to write down a definition for the polyhedron that is used to produce  $G_\theta$ . When  $\theta < 2\pi$  we take six circles of radius  $r_\theta$  with centres  $\epsilon r + \delta 2ri$  where  $\epsilon \in \{\pm 1\}$ ,  $\delta \in \{-1, 0, 1\}$ , and two circles of radius  $r_\theta$  centred at  $\pm r_\theta i$ . These, together with the four lines  $\pm 1/2 + \mathbb{R}i$  and  $\mathbb{R} \pm 2ri$  define a hyperbolic polyhedron with 14 hyperbolic faces and four ideal faces on the Riemann sphere. It has two edges of dihedral angle  $\pi$ , namely the intersections of domes with the hyperbolic plane lying above the real axis, and all other edges have dihedral angle  $\pi/2$  except for those arising as intersections of domes with the two planes above the vertical lines  $\pm 1/2 + \mathbb{R}i$ . There are four of these latter type of edges which each have dihedral angle  $\theta/4$ . When  $\theta \rightarrow 2\pi$  this polyhedron degenerates to the polyhedron for the Borromean rings given in Figure 5(B) and when  $\theta \rightarrow 0$  it degenerates to the polyhedron given in Figure 6(B). Since it is combinatorially identical to the latter, we define side-pairings by writing down the uniquely defined Möbius transformations which pair the faces in the same combinatorial pattern as in that group (i.e. the pattern of Table 2).

The result then follows from a cone manifold version of the Poincaré polyhedron theorem, for instance the version described in Appendix A, as an exercise in checking that all edge sums add to  $2\pi$ , except for a single edge cycle which has angle sum  $\theta$ . By our choice of the embedding of the polyhedron in  $\mathbb{H}^3$  (e.g. choosing the horizontal width of the rectangle to be 1) these transformations will obey the normalisations that we imposed earlier and so will interpolate directly between  $G_0$  and  $G_{2\pi}$ .  $\square$

### 3. STACKED BORROMEAN RINGS AND LANTERN MANIFOLDS

As described in the introduction, for our applications to 2-bridge links we will be interested in manifolds where the two rank 2 cusps in the lantern manifold are replaced with  $2n$  cusps (for some  $n \in \mathbb{N}$ ) that interleave as in Figure 8. We call this the *n*-stacked lantern manifold, denoted  $M^n$ . Gluing a 2-handle along the dotted curve in the figure produces the complement  $B^n$  of the  $n$ -stacked Borromean rings  $\mathfrak{b}^n$ . For completeness, we give a formal definition of  $M^n$  and  $\mathfrak{b}^n$ :

FIGURE 9. The components of the stacked Borromean rings,  $b^n$ .

**Definition 3.1.** The  $n$ -stacked Borromean rings is the link  $b^n \subset \mathbb{S}^3$  with a diagram in  $\mathbb{R}^2$  produced by the following algorithm; compare with Figure 9.

- (1) Draw rectangles  $\mu_1, \dots, \mu_n$ , where  $\mu_i$  is determined by the diagonally-opposite corners  $(-i, -i + 1/2)$  and  $(i, i - 1/2)$ .
- (2) Draw rectangles  $\alpha_1, \dots, \alpha_n$ , where  $\alpha_i$  is determined by the diagonally-opposite corners  $(-i + 1/2, -n - i/2)$  and  $(i - 1/2, n + i/2)$ .
- (3) At all crossing points  $(x, y)$  between any  $\mu_i$  and  $\alpha_j$ , if  $y < 0$  then define  $\mu_i$  to cross over  $\alpha_j$  and if  $y > 0$  then define  $\alpha_j$  to cross over  $\mu_i$ .
- (4) Draw a rectangle  $\chi$  determined by the diagonally-opposite corners  $(-n - 1/2, -n)$  and  $(n + 1/2, n)$ .
- (5) At all crossing points  $(x, y)$  between  $\chi$  and some  $\alpha_j$ , if  $x < 0$  then  $\chi$  crosses over  $\alpha_j$  and if  $x > 0$  then  $\alpha_j$  crosses over  $\chi$ .

The *central component* is the component represented by the loop  $\chi$ . The  $n$ -stacked lantern manifold is the topological manifold  $M^n$  obtained by adding the arc which we will now describe to the diagram of  $b^n$ , lifting the result into  $\mathbb{S}^3$  as an embedded graph, and taking the complement of this graph.

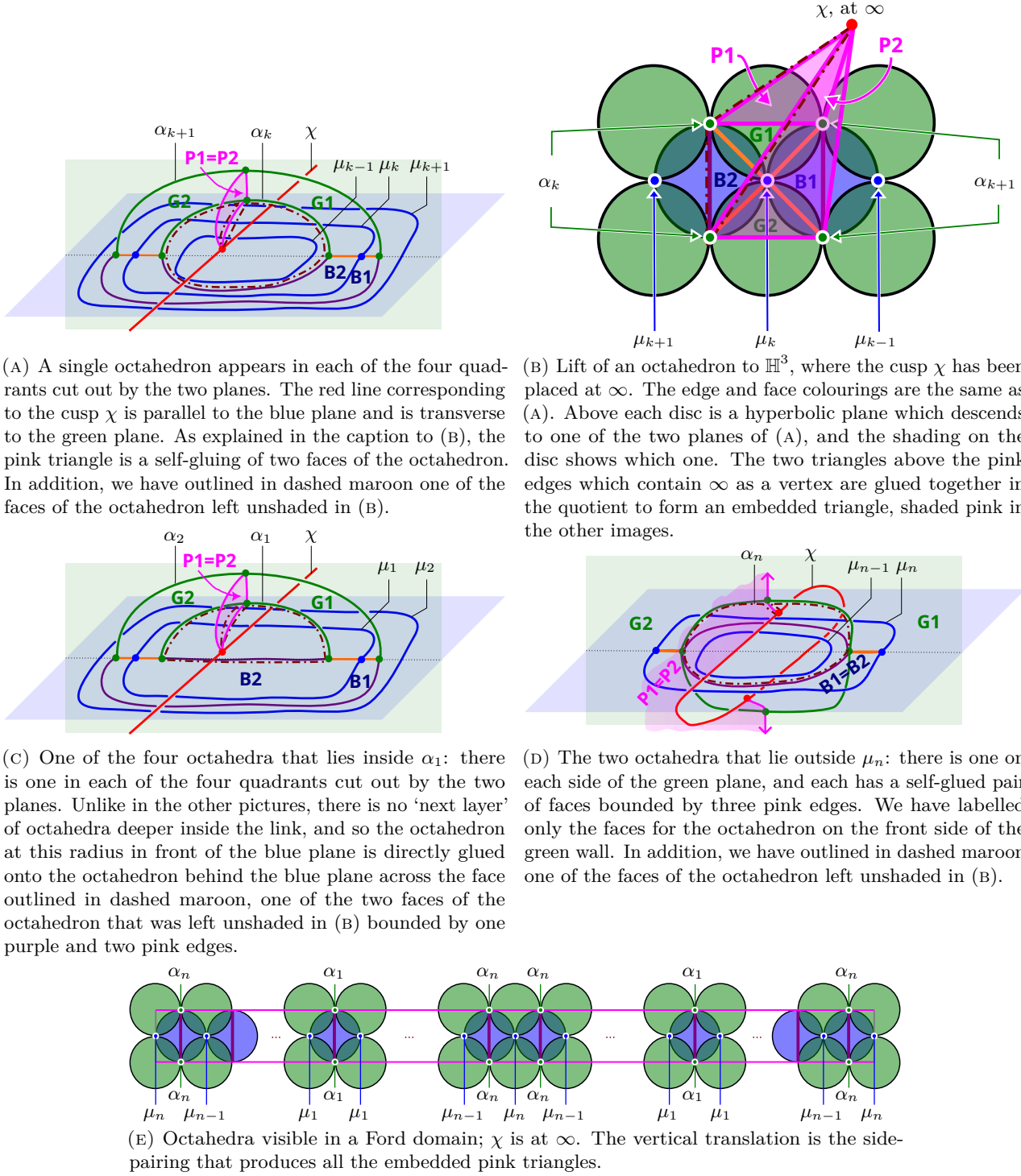
- (6) Draw a vertical segment  $\tau$  between  $(0, -n)$  and  $(0, n)$ . This segment meets  $\chi$  at its two endpoints, which are trivalent vertices of the graph. All other crossing points  $(x, y)$  between  $\tau$  and a component of the diagram are incidences between  $\tau$  and some  $\mu_j$ ; if  $y > 0$  then  $\tau$  crosses over the strand  $\mu_j$ , and if  $y < 0$  then  $\tau$  crosses under  $\mu_j$ .

See Figure 3(A) in the introduction for an example of such a diagram for  $n = 3$ .

**3.1. Hyperbolic structure.** Just as for the lantern group, we could set up and solve a system of polynomial equations in the entries of generators for the image of  $\pi_1(M^n)$  in  $\text{PSL}(2, \mathbb{C})$ . However, the number of variables grows with  $n$  and there is not much geometric enlightenment to be gained from the algebra. Instead, we construct the hyperbolic structures by triangulating  $B^n$  and then carrying out a cone deformation similar to that of Proposition 2.4 to construct a fundamental domain for  $M^n$ .

**Theorem 3.2.** Let  $b^n$  be the  $n$ -stacked Borromean rings, and let  $B^n = \mathbb{S}^3 \setminus b^n$ . Then  $B^n$  admits a complete hyperbolic structure that decomposes as a union of  $4n - 2$  ideal right-angled octahedra.

*Proof.* The 2-sphere  $S$  in  $\mathbb{S}^3$  containing all the cusps  $\mu_j$  (the blue plane of Figure 9) can be divided into a union of  $n - 1$  four-punctured spheres and 2 thrice-punctured spheres; a pair of adjacent four-punctured spheres in this decomposition is shown in Figure 10(A). In the same figure, we show the construction of a single octahedron, with one vertex at  $\infty$ , one each at the cusps  $\mu_{k-1}$ ,  $\mu_k$ , and  $\mu_{k+1}$ , and four remaining vertices coming from meeting each of the two cusps  $\alpha_k$  and  $\alpha_{k+1}$  twice. This octahedron lifts to  $\mathbb{H}^3$  as shown in Figure 10(B). These octahedra cover the entire link complement, except for a piece inside the cusp  $\mu_1$  and a piece outside the cusp  $\mu_n$ . The region inside  $\mu_1$  is formed from a gluing of four octahedra as in

FIGURE 10. Octahedral decomposition of  $B^n$ .

**Figure 10(C).** The region outside  $\mu_n$  is formed from a single pair of octahedra which glue up around the  $\mu_n$  cusp as in **Figure 10(D).**

In total, we obtain a set of  $4n - 2$  octahedra which lift as shown in **Figure 10(E).** The rectangle is a fundamental domain for the central cusp of  $\mathfrak{b}^n$ , i.e. the cusp  $\chi$ .

The other circles shown are all of equal radius, and the intersection points of these circles are the lifts of cusps as labelled.

This combinatorial polyhedron can be metrically realised in  $\mathbb{H}^3$  with all ideal vertices and all angles  $\pi/2$  or (at adjacency between two octahedra)  $\pi$ . It can be checked that in the decomposition of  $B^n$  every edge is surrounded by 4 octahedra; thus all angle sums around edges are  $2\pi$ . In addition the transformations pairing tangent circles can be chosen to be parabolic. These observations verify the hypotheses of the Poincaré polyhedron theorem and so this ideal triangulation defines a complete hyperbolic structure.  $\square$

As a straightforward consequence of [Theorem 3.2](#) we see that the links  $\mathfrak{b}^n$  are arithmetic [[37](#), Lemma 3.2] with invariant trace field  $\mathbb{Q}(i)$ , and the manifolds  $B^n$  have hyperbolic volume  $(32n - 16)\Pi(\pi/4)$  where  $\Pi$  is the Lobachevsky function [[43](#), §7.2]. More important to our applications is the following additional corollary.

**Corollary 3.3.** *The cusp shapes of  $B^n$  (i.e. the Euclidean length of the longitude when the meridian is normalised to length 1) are:  $4n - 2$  for  $\chi$ ; 2 for  $\alpha_1$  and  $\mu_n$ ; and 1 for all other cusps.*

*Proof.* For an ideal regular octahedral decomposition, the cusp shape can be computed as the ratio between the number of polyhedral walls crossed while walking around the longitude of each cusp to the number of walls crossed while walking around the meridian. This is carefully explained in Futer and Purcell [[18](#), §2.2]. As an example, consider the cusps  $\alpha_k$ . When  $k > 1$ , the incident octahedra are as shown in [Figure 10\(A\)](#). Walking around the intersection point of  $\alpha_k$  in the horizontal plane  $S$ , we meet an orange edge (joining  $\alpha_k$  to  $\alpha_{k+1}$ ), a purple edge (joining  $\alpha_k$  to  $\alpha_k$ ), a second orange edge (joining  $\alpha_k$  to  $\alpha_{k-1}$ ), and a second purple edge (joining  $\alpha_k$  to  $\alpha_k$ ), so in walking around the meridian of the cusp four octahedra walls are passed. Walking around the longitude one passes through only two octahedra, but there are two additional walls (pink) that correspond to a self-gluing of an octahedron, so the total is still 4 and the cusp shape is  $4/4 = 1$ . When  $i = 1$ , the incident octahedra are as shown in [Figure 10\(C\)](#); there are still 4 octahedra along the longitude, but when walking along the meridian one only passes through two walls, giving a cusp shape of  $4/2 = 2$ .  $\square$

**Construction 3.4.** The fundamental domain shown in [Figure 10\(E\)](#) has a single vertex that descends to  $\chi$ , which is placed at  $\infty$ , and has 4 vertices which descend to  $\alpha_1$ . We will rearrange the component octahedra so that there is a single vertex which descends to  $\alpha_1$ , and we will move it by isometry in  $\mathbb{H}^3$  so that this single vertex is at  $\infty$ .

Consider the rectangle of [Figure 10\(E\)](#) which gives a fundamental domain for the stabiliser of  $\infty$ ; it is superimposed on top of a pair of dual circle packings of the plane. We may translate the rectangle around on these circle packings arbitrarily, and the resulting figure will still define a fundamental domain. Translate it so that one of the points descending to  $\alpha_1$  is the centre of reflective symmetry. The resulting domain has 3 vertices which descend to  $\alpha_1$ , which are the points of tangency of the six shaded circles in [Figure 11\(A\)](#). Without loss of generality, the central point descending to  $\alpha_1$  is  $0 \in \mathbb{C}$  and the grey dotted circle shown in [Figure 11\(A\)](#) (defined by being centred at 0 and tangent to the four circles meeting there) is the unit circle. We also distinguish two vertical lines (black dotted in the figure), namely the vertical lines through the lifts of  $\mu_n$ .

Apply the hyperbolic isometry  $z \mapsto 1/z$ ; this is a circle inversion in the unit circle followed by reflection in the horizontal line of symmetry, and the result is shown in [Figure 11\(B\)](#). This has the effect of moving the vertex corresponding to  $\chi$  to 0, and moving a vertex corresponding to  $\alpha_1$  to  $\infty$ .

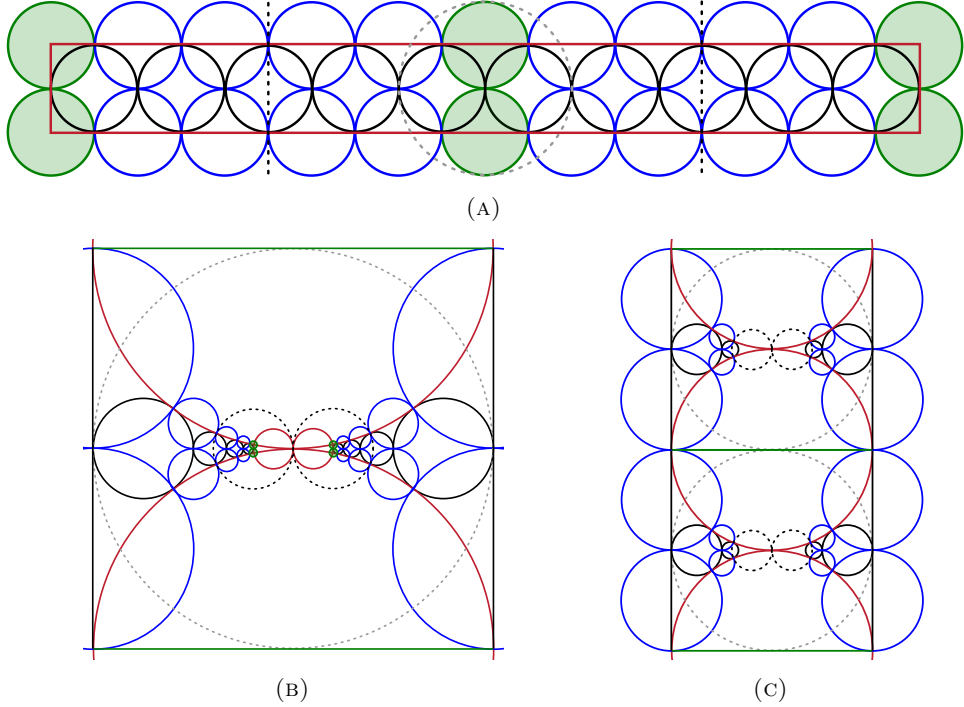


FIGURE 11. Cutting and gluing in Construction 3.4.

Finally, cut along the hyperbolic planes above the black dotted circles and glue these pieces along the inverts of the green circles, to form a rectangle of aspect ratio  $2 : 1$  as in Figure 11(C); this is a rearrangement of the octahedra making up the fundamental domain so that the cusp  $\alpha_1$  is represented by a single vertex. In the resulting domain the cusp  $\chi$  is represented by two vertices.

The domain which results from Construction 3.4 can be compared with the horoball view of the 3-stacked Borromean rings displayed in Figure 3(B).

**Theorem 3.5.** *There exists a path in the character variety of  $M^n$  parameterising hyperbolic cone manifold holonomy groups in which  $ZY^{-1}$  changes from a parabolic, through elliptics of increasing holonomy angle from  $0$  to  $2\pi$ , to the identity; at each point the cone manifold is obtained by filling the  $ZY^{-1}$  cusp with an ideal cone arc of the appropriate angle, and the path limits onto  $B^n$ . This deformation preserves all cusp shapes except for that of the cusp  $\alpha_1$  which, in the limit, has normalised longitude  $2n - 1$ .*

*Proof.* Consider a fundamental domain for  $B^n$  as constructed in Construction 3.4; the vertical line of symmetry of this figure cuts the two vertices that descend to the cusp we wish to remove. Just as in Proposition 2.4, we may cut along this line and pull the two halves apart, introducing a new quadrilateral ideal face where each of these vertices was. This corresponds to increasing the translation length of the horizontal Euclidean transformation. The geometry around no other edge is affected, so all other edge-cycles remain unchanged and the group defined by the side-pairings of the new polyhedron is the holonomy group of a hyperbolic polyhedron with the same cusp shapes and combinatorics, the only difference being a new elliptic arc joining the two new thrice-marked spheres at infinity. In particular all cusp shapes remain the same since relative sizes of isometric circles of parabolics are preserved (the pairs of circles are simply shifted by an appropriate Euclidean translation).  $\square$

*Remark 3.6* (The limits  $B^\infty$  and  $M^\infty$ ). Two examples of non-free infinitely generated Kleinian groups arise as limiting cases. Indeed, the Poincaré polyhedron theorem holds for polyhedra in  $\mathbb{H}^3$  with countably many faces, so long as ideal vertices are locally finite; see [Appendix A](#). As  $n \rightarrow \infty$ , the polyhedra of [Construction 3.4](#) have a well-defined limit, and this limit satisfies the conditions of the polyhedron theorem: the face-pairings generate discrete groups and in each case the polyhedron glues to give a complete hyperbolic metric of infinite volume on the quotients  $M^\infty$  and  $M^\infty$ .

The group  $\text{Hol}(B^\infty)$  includes a rank 1 parabolic subgroup which is not doubly cusped. The group  $\text{Hol}(M^\infty)$  includes a pair of thrice-punctured sphere groups which share two conjugacy classes of maximal rank 1 parabolic subgroups; these groups are doubly cusped. The third puncture of each thrice-punctured sphere is represented by a rank 1 parabolic group that is not doubly cusped.

**3.2. Dehn filling.** The Gromov–Thurston  $2\pi$ -theorem, see Bleiler and Hodgson [5, Theorem 9], states that if  $M$  is a complete hyperbolic 3-manifold with finite volume then a sufficient condition for a Dehn filling of  $M$  to be negatively curved is that the Euclidean length of the geodesic representing each slope is at least  $2\pi$ . With this machinery, we may deduce the following result. The final statement on geodesicity of the unknotting tunnel has been proved in general by Adams and Reid [2, Theorem 3.2] using different techniques.

**Theorem 3.7.** *Let  $\mathfrak{k}$  be a 2-bridge knot so that the slope of  $\mathfrak{k}$  has continued fraction decomposition  $[2m_n, 2a_n, \dots, 2m_1, 2a_1]$ . If  $m_n \geq 4$  and  $a_n, m_{n-1}, \dots, m_1, a_1 \geq 7$ , then there is a continuous family of cone manifolds  $M_\theta$ ,  $\theta \in (0, 2\pi]$  supported on the link complement  $\mathbb{S}^3 \setminus \mathfrak{k}$  with singular locus consisting exactly of an ideal cone arc along the upper unknotting tunnel of  $\mathfrak{k}$ . The limit as  $\theta \rightarrow 0$  is well-defined, and is a maximal cusp point on the boundary of genus 2 Schottky space. The upper unknotting tunnel of  $\mathfrak{k}$  is isotopic to a geodesic in the complete hyperbolic structure on  $\mathbb{S}^3 \setminus \mathfrak{k}$ .*

*Proof.* Suppose that  $\mathfrak{k}$  has slope  $p/q$ . Consider a genus 2 handlebody  $\mathcal{H}$ ; let  $\sigma_1$  and  $\sigma_2$  be projections to the genus 2 surface  $\partial\mathcal{H}$  of the cores of the two handles. Then  $S = \partial\mathcal{H} \setminus (\sigma_1 \cup \sigma_2)$  is a four-holed sphere. Let  $\tau$  be the simple closed curve on  $S$  with homology class  $p\gamma_{1/0} + q\gamma_{0/1}$ , where  $\gamma_{1/0}$  is the homology of the curve on  $S$  bounding a compression disc in  $\mathcal{H}$  and where  $\gamma_{0/1}$  is a curve which intersects  $\gamma_{1/0}$  exactly twice; c.f. Farb and Margalit [17, §2.2.5]. Then  $\mathbb{S}^3 \setminus \mathfrak{k}$  is the manifold obtained by gluing a 2-handle onto  $\mathcal{H}$  along  $\tau$ . In addition, the continued fraction decomposition  $[2m_n, 2a_n, \dots, 2m_1, 2a_1]$  encodes the sequence of Dehn twists of the four-punctured sphere which produce  $\tau$  from  $\gamma_{0/1}$ . There is a hyperbolic 3-manifold  $N$  on the boundary of genus 2 Schottky space which is homeomorphic to  $\mathcal{H}$  and which has rank 1 cusps represented by the three loops  $\sigma_1$ ,  $\tau$ , and  $\sigma_2$ . Consider now the lantern manifold  $M^n$ . If we Dehn fill  $M^n$  by  $1/a_i$  filling the cusps  $\alpha_i$  and  $1/m_j$  filling the cusps  $\mu_j$  then we obtain  $N$ : indeed, the various Dehn fillings of slope  $1/a_i$  (resp.  $1/m_j$ ) just perform  $a_i$  (resp.  $m_j$ ) Dehn twists along  $\gamma_{1/0}$  (resp.  $\gamma_{0/1}$ ). The point is that  $N$  is obtained by drilling the upper unknotting tunnel from  $\mathbb{S}^3 \setminus \mathfrak{k}$  and the loop  $\tau$  is the meridian of the unknotting tunnel. By the  $2\pi$ -theorem, and using the cusp shapes computed in [Theorem 3.5](#), the filling is hyperbolic whenever the conditions in the theorem statement are satisfied. Explicitly,  $\sqrt{1 + (2n)^2} > 2\pi$  if and only if  $n \geq 4$  and  $\sqrt{1 + n^2} > 2\pi$  if and only if  $n \geq 7$ .

Next, we note that the proof of the  $2\pi$  theorem given by Bleiler and Hodgson [5, Theorem 9] works without change for cone manifolds: it relies only on a lemma of Gromov (Lemma 10 *op. cit.*) which fills in the hyperbolic metric on the interior of a solid torus to extend a hyperbolic metric on a neighbourhood of the boundary, and this is independent of whether there are singular arcs away from the horoball

being filled. It is also clear from the proof of this lemma that the metric in the filled horoball is continuous with respect to the metric near the boundary, so continuous variation of the metric in the manifold being filled will induce a continuous metric on the filled manifolds.

Now we can put these observations together: if  $M_\theta^n$  is the cone manifold obtained by cone-deforming  $M^n$  using [Theorem 3.5](#) so that the cone arc has angle  $\theta$ , then we can use the  $2\pi$  theorem to Dehn fill it and obtain a cone manifold  $N_\theta$  supported on  $\mathbb{S}^3 \setminus \mathfrak{k}$  with a cone arc of angle  $\theta$  along the upper unknotting tunnel. In the limit as  $\theta \rightarrow 2\pi$  we obtain the complete hyperbolic metric on  $\mathbb{S}^3 \setminus \mathfrak{k}$  as a Dehn filling of  $M_{2\pi}^n = B^n$ . By continuity of the metric, the unknotting tunnel of  $\mathfrak{k}$  was isotopic to a geodesic (the axis of an elliptic element) in  $N_\theta$  for all  $\theta < 2\pi$  and so it remains as such in  $N_{2\pi} = \mathbb{S}^3 \setminus \mathfrak{k}$ , proving the final statement of the theorem.  $\square$

*Remark 3.8.* In 2000, Agol [3] and Lackenby [30] showed that, in the presence of the Thurston Geometrisation Theorem proved by Perelman [35; 36], the bound  $2\pi$  can be improved to 6; this result is called the 6-theorem, and would allow the bounds in [Theorem 3.7](#) to be slightly improved from 7 and 4 to 6 and 3 respectively. However, the presence of the geometrisation theorem in this improvement means that our naïve approach fails. Indeed, we rely on being able to modify the proof of the  $2\pi$ -theorem to work for hyperbolic cone manifolds; one would first argue that by the 6-theorem the cone manifold holonomy groups are word-hyperbolic, but then we cannot apply geometrisation as a black box to deduce that the cone manifolds are in fact hyperbolic. The proof of geometrisation for 3-orbifolds given by Boileau, Leeb, and Porti [6] holds for cone manifolds with cone arcs of angle in  $[0, \pi]$ , but does not hold in  $(\pi, 2\pi]$  and cannot be improved in general as it relies on the global rigidity results of Hodgson and Kerckhoff [24] which fail in general in this domain (as discussed in the introduction).

Replacing the stacked Borromean rings with a slightly different link, we can obtain a version of [Theorem 3.7](#) for links of two components. We will only provide a sketch of the proof as it requires no new ideas. The final statement on geodesicity of the unknotting tunnel has been proved in general by Adams [1, Lemma 4.6] using different techniques.

**Proposition 3.9.** *Let  $\mathfrak{k}$  be a 2-bridge link with 2 components whose slope has continued fraction decomposition  $[2m_n, 2a_n, \dots, 2m_1]$ . If  $m_n \geq 4$  and  $a_n, m_{n-1}, \dots, m_1 \geq 7$ , then there is a continuous family of cone manifolds  $M_\theta$ , parameterised by  $\theta \in (0, 2\pi]$ , supported on the link complement  $\mathbb{S}^3 \setminus \mathfrak{k}$  and with singular locus consisting exactly of an ideal cone arc of angle  $\theta$  along the upper unknotting tunnel of  $\mathfrak{k}$ . The limit as  $\theta \rightarrow 0$  is a maximal cusp point on the boundary of genus 2 Schottky space and the upper unknotting tunnel of  $\mathfrak{k}$  is isotopic to a geodesic in the complete hyperbolic structure on  $\mathbb{S}^3 \setminus \mathfrak{k}$ .*

*Proof.* Take the central component of  $\mathfrak{b}^n$  and split it into two loops,  $\chi_1$  and  $\chi_2$ , as in [Figure 12\(A\)](#); the component  $\alpha_1$  is now be homotopic to a point, and so we throw it away. The complement of this link in  $\mathbb{S}^3$  has an octahedral decomposition which can be found, just as in [Theorem 3.2](#), by placing one of the two central cusps at  $\infty$ ; the cusp shape of each central cusp is now  $(2n - 2)$  rather than  $(4n - 2)$ , and the arrangement of the octahedra is exactly the same as in the stacked Borromean rings except for the inner four octahedra which are replaced by a pair of octahedra glued to ‘wrap around’ just like the outer pair of octahedra—we show these two octahedra in [Figure 12\(C\)](#). If the cusp  $\mu_1$  to is moved to  $\infty$  then we end up with an aspect ratio  $2 : 1$  rectangle as in [Figure 12\(D\)](#). Just as in [Theorem 3.5](#) this fundamental domain can be modified continuously to ‘pull apart’ the two parabolic fixed points corresponding to the two central cusps of the link; this cone-deforms

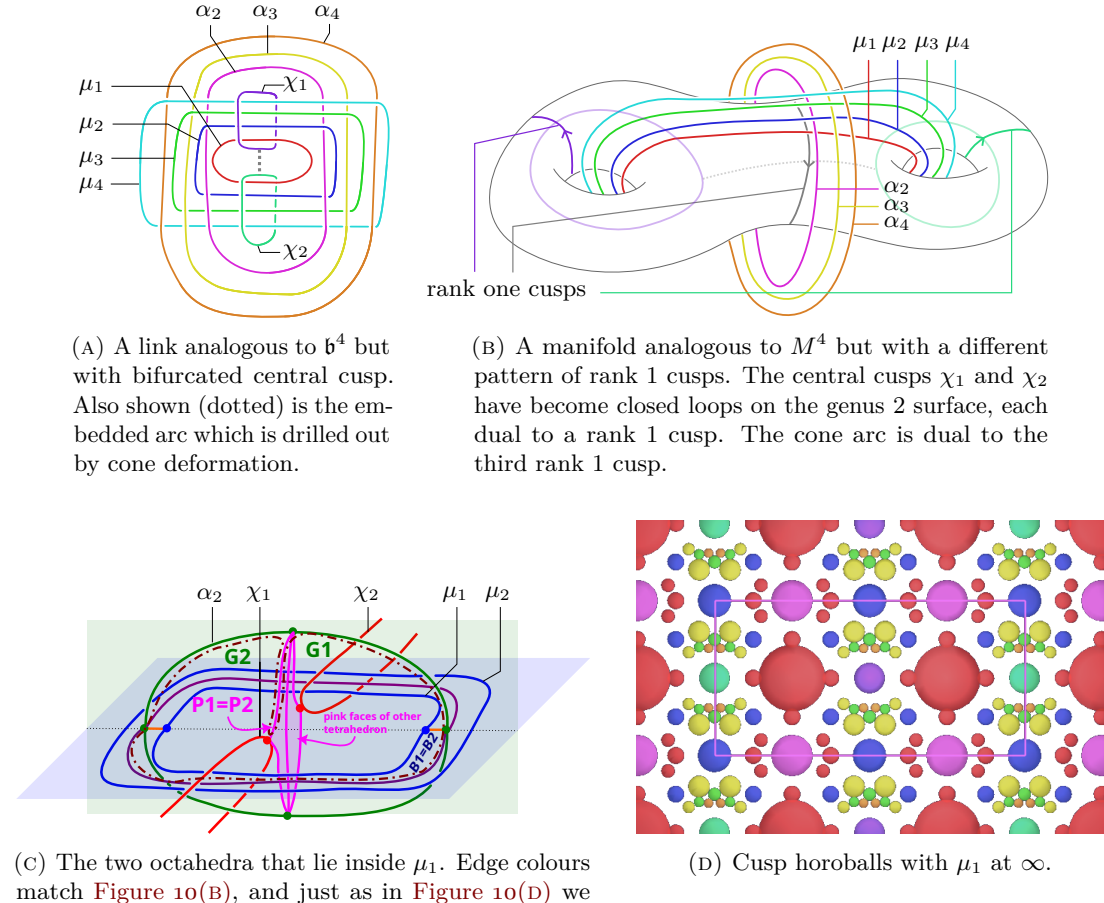


FIGURE 12. The manifolds analogous to  $B^n$  and  $M^n$  that can be used to study 2-component links.

the link in Figure 12(A) to the manifold in Figure 12(B) with  $2n - 1$  rank two cusps and conformal boundary consisting of two thrice-punctured spheres glued along rank 1 cusps along the indicated curves. Running through the proof of Theorem 3.7 with this new setup gives the result.  $\square$

#### 4. CONCAVE LENSES AND OTHER EXPANSION JOINTS

We isolate the substructure of the manifold which makes the arguments in the previous sections work.

**Definition 4.1.** A *concave lens* is a polyhedral complex made up of  $n$  distinct octahedra  $C_1, \dots, C_n$  that all share a vertex  $v$  and so that  $C_{i-1} \cap C_i$  and  $C_i \cap C_{i+1}$  (subscripts taken modulo  $n$ ) are 2-faces that intersect only at  $v$ . Roughly speaking, the 1-skeleton of the complex is a cycle that does ‘not turn any corners’. The *outer vertices* of the lens are the  $n$  vertices that do not lie in faces incident with  $v$ . The *inner faces* are the  $2n$  boundary faces that are incident with  $v$ . The *rim faces* are the  $2n$  faces that meet an outer vertex and do not meet an inner face.

In Figure 13 we show a concave lens with  $n = 8$ . We will now give some conditions on a concave lens embedded in a manifold that will allow it to act as an expansion joint in the sense we described in the introduction: the longitude of the central cusp

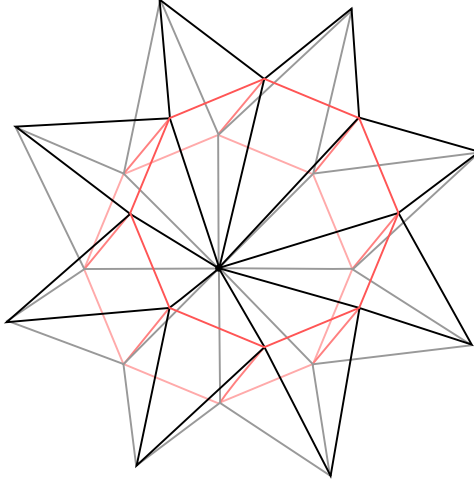


FIGURE 13. Concave lens of 8 octahedra.

can be elongated, producing gaps in the polyhedral decomposition of the manifold around the opposite vertices, while preserving the conformal structure of ends not adjacent to the lens.

**Theorem 4.2.** *Let  $M$  be a hyperbolic 3-manifold with convex core  $K(M)$  decomposed as a polyhedral complex  $\mathcal{C}$ . Let  $v$  be an ideal vertex of  $\mathcal{C}$  that models a rank 2 cusp of  $M$ , and let  $\hat{\mathcal{C}}$  be a connected lift of  $\mathcal{C}$  to the universal cover of  $K(M)$  so that  $v$  lifts to a single vertex. Let  $\sim$  be the equivalence relation on  $\hat{\mathcal{C}}$  induced by the quotient projection. Suppose that  $\hat{\mathcal{C}}$  contains an embedded concave lens  $\mathcal{L}$  made up of ideal octahedra, with central vertex  $v$ , satisfying the following properties:*

- (1) *The outer vertices of  $\mathcal{L}$  are lifts of rank 2 cusps of  $M$ .*
- (2) *The  $\sim$ -class of each outer vertex of  $\mathcal{L}$  consists only of outer vertices of  $\mathcal{L}$ .*
- (3) *The  $\sim$ -class of each rim face of  $\mathcal{L}$  consists only of rim faces of  $\mathcal{L}$ .*
- (4)  *$\mathcal{L}$  is symmetric under reflection in a geodesic plane that contains  $v$  and all the outer vertices.*

*Then there exists a smooth path  $M_\theta$  of cone manifolds, parameterised by  $\theta \in (0, 2\pi]$  consisting of hyperbolic cone manifolds that are supported on the topological manifold  $M_{2\pi} = M$  and where the cone arcs in  $M_\theta$  join the outer vertices of  $\mathcal{L}$  along the rim faces. If  $M$  has any conformal ends, then their conformal structure is preserved by the deformation, and the shapes of rank 2 cusps that do not meet  $\mathcal{L}$  are preserved.*

*Remark 4.3.* We have arranged all images of cusp horoballs in this paper so that the outer cusps from the relevant concave lens appear along the horizontal line of symmetry. This means that the central plane of symmetry of the cusp is the hyperbolic plane through  $\infty$  supported on this horizontal line, and the cone arcs appear along this line (c.f. Figure 3(B)).

To prove [Theorem 4.2](#), we will need the following standard lemma.

**Lemma 4.4.** *Let  $\Lambda$  be a rank 2 lattice. If  $f \in \Lambda$  is primitive, i.e. if whenever there exist  $n \in \mathbb{N}$  and  $g \in \Lambda$  with  $n \cdot g = f$  then  $n = 1$  and  $g = f$ , then  $\{f\}$  may be extended to a basis of  $\Lambda$ .  $\square$*

*Proof of Theorem 4.2.* Choose a fundamental domain for  $M$  consisting of a lift  $\hat{\mathcal{C}}$  of  $\mathcal{C}$  to  $\mathbb{H}^3$ . By an appropriate isometry we may assume that  $v$  lifts to  $\infty$ . Let  $f$  be the element of  $\text{Hol}(M)$  corresponding to the closed around  $v$  in the concave

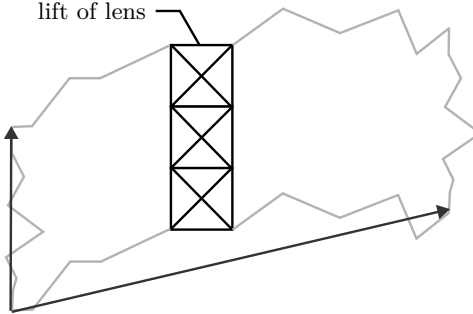


FIGURE 14. Lift to  $\mathbb{H}^3$  of a manifold containing a concave lens made up of ideal regular octahedra.

lens octahedra; without loss of generality,  $f$  is a vertical translation, along the  $y$ -axis. Since the lens is embedded,  $f$  is a primitive element of the rank 2 lattice  $\text{Stab}_{\text{Hol}(M)}(\infty)$  and hence by [Lemma 4.4](#) we can choose a generating set for this lattice containing  $f$ .

The fundamental domain for  $M$  coarsely looks like [Figure 14](#); since the lens is embedded, there are no vertices of the complex  $\hat{C}$  lying above the rectangular projection of the lens octahedra to the Riemann sphere other than  $\infty$  (but it is possible for other vertices to lie below, as seen for instance in [Figure 11\(c\)](#) above). Just as in [Theorem 3.5](#) we may now horizontally pull apart the two halves of this rectangular projection, without changing the combinatorial or geometric structure of any other part of  $\hat{C}$  (in particular, we preserve all angle sums away from the lift of the lens). All cusp shapes remain constant except for the shape of the cusp at  $\infty$ ; the translation vector of  $f$  remains constant, while the translation vector of the other basis element of  $\text{Stab}_{\text{Hol}(M)}(\infty)$  is skewed (the component parallel to the translation vector of  $f$  remains constant and the orthogonal component increases in length by exactly the width of the rectangular projection of the lens octahedra).  $\square$

**4.1. Fully augmented links.** We present a family of examples realising [Theorem 4.2](#), arising from fully augmented links. The components of a fully augmented link are separated into *augmentation cusps* (also known as *crossing circles*) which each bound twice-punctured discs normal to some plane of reflective symmetry, and *planar cusps* (also known as *knot strands*) that lie in the reflection plane; for more information see Purcell [40]. Every planar cusp in a fully augmented link bounds two multiply-punctured discs in the reflection plane.

**Theorem 4.5.** *Let  $\mathfrak{l}$  be a fully augmented link with a planar cusp  $\omega$  such that:*

- (i) *There are no self-augmentations of  $\omega$  (i.e. no augmentation cusp bounds a disc that meets  $\omega$  twice), and*
- (ii) *One of the two discs,  $D$ , bounded by  $\omega$  in the reflection plane of  $\mathfrak{l}$  must be punctured only by augmentation cusps.*

*Then  $\omega$  forms the centre of a concave lens satisfying the conditions of [Theorem 4.2](#), and increasing the longitudinal length of  $\omega$  forms cone arcs in the geodesic surface  $D$  joining the augmentation cusp punctures together.*

The proof will be illustrated using the fully augmented link in [Figure 15\(A\)](#).

*Proof.* We will decompose the link  $\mathfrak{l}$  using the so-called *method of chequerboards*; we assume that the reader is somewhat familiar with this procedure, which is originally described in the appendix by Agol and Thurston to Lackenby [29] and which is further explained in [18; 21; 26; 40].

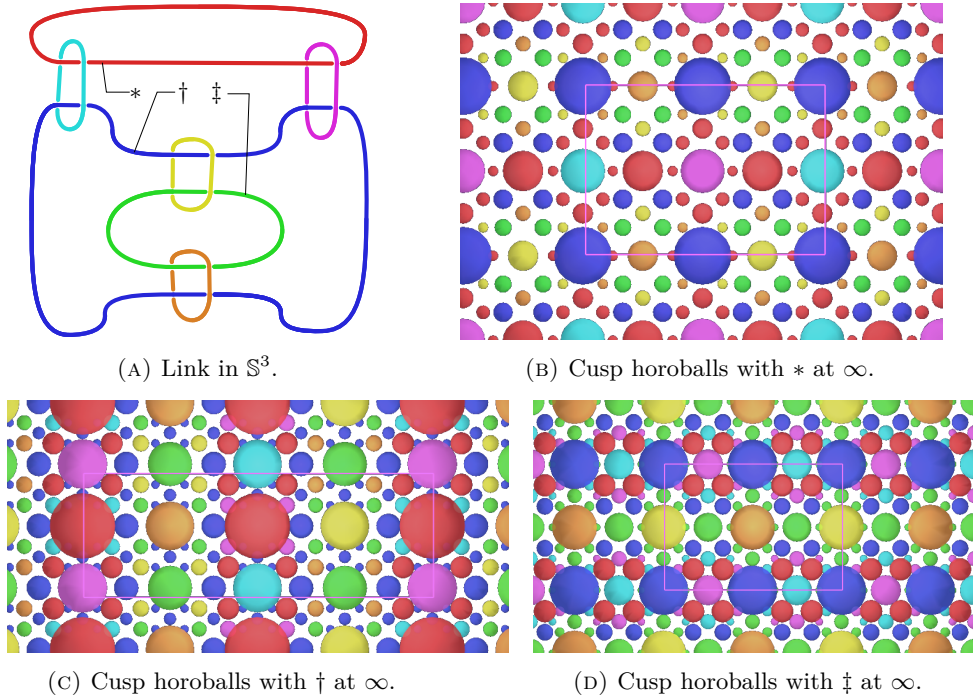
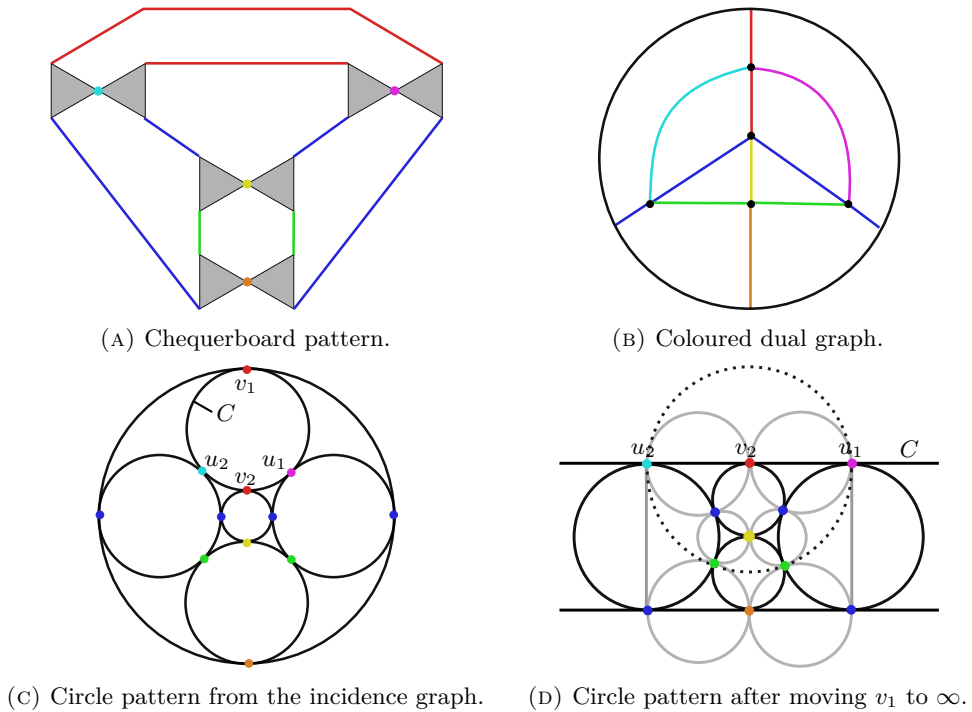


FIGURE 15. An octahedral fully augmented link.

FIGURE 16. The circle pattern arising from the link in Figure 15, illustrating the proof of Theorem 4.5. The red vertices, corresponding to the cusp  $*$ , will be combined and form the central vertex  $v$ .

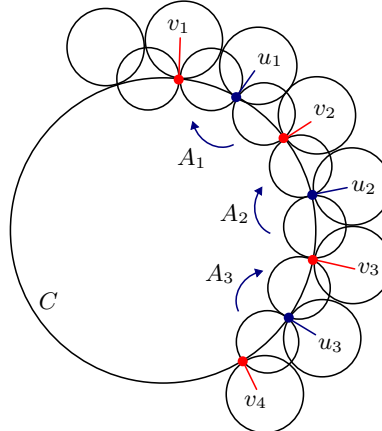


FIGURE 17. Notation for proof of Theorem 4.5.

Let  $\Pi$  be the reflection plane of  $\mathfrak{l}$ . Cutting along  $\Pi$  and then cutting along each thrice-punctured sphere transverse to  $\Pi$  produces a chequerboard pattern as in Figure 16(A) (compare Figure 2 of [40]). Contract each triangle into a vertex and interpret each rank 1 cusp as an edge. This gives a trivalent graph  $\Gamma$  together with an edge-colouring, a map  $\chi : E(\Gamma) \rightarrow \text{Cusps}(\mathfrak{l})$ . The conditions (i) and (ii) imply that there is a simple edge-cycle  $e_1, \dots, e_r$  in  $\Gamma$  such that:

- (1) If  $i$  is odd, then  $\chi(e_i) = \omega$ ; conversely, if  $\chi(e) = \omega$  for any  $e \in E(\Gamma)$ , then  $e = e_i$  for some odd  $i$ , and
- (2) If  $e \in E(\Gamma)$  and  $\chi(e) = \chi(e_i)$  for some  $e_i$ , then  $e = e_j$  for some  $j$ .

For instance, in Figure 16(A) there is a loop with red edges (corresponding to the cusp  $\ast$ ) alternating with edges of different colours, and the total set of colours in this loop appears nowhere else in the edge colouring.

Take the dual graph of  $\Gamma$  (Figure 16(B)) and construct the circle pattern  $P$  with tangency arrangement given by the graph (Figure 16(C)); tangency points inherit the colouring map  $\chi$ . This circle pattern has a dual pattern  $P^\perp$  of orthogonal circles; take the right-angled polyhedron in  $\mathbb{H}^3$  bounded by the domes above the circles in the pattern and above the dual circles, and two copies of this polyhedron glue to give  $\mathbb{S}^3 \setminus \mathfrak{l}$ : the domes above the dual circles in  $P^\perp$  are in correspondence with the triangular faces of the chequerboard pattern and glue in pairs to form halves of the discs bounded by augmentation cusps, and the domes above our original circles in  $P$  glue across  $\Pi$  onto the corresponding faces of the second copy of the polyhedron.

From our discussion above, there is a distinguished circle  $C$  in  $P$  so that the points of tangency around its circumference alternate between points descending to  $\omega$  and points which do not. Let  $D$  be one of the two right-angled ideal polyhedra just constructed and pick a vertex of  $D$  that descends to  $\omega$ , say  $v_1$ . Then label all the vertices of  $D$  around  $C$  as  $v_1, u_1, v_2, u_2, \dots, v_n, u_n$  where each  $v_i$  descends to  $\omega$ . By the discussion of the face-pairing structure on  $D$  in the previous paragraph, each  $u_i$  is the point of tangency of two faces of  $D$ , orthogonal to  $C$ , paired by a parabolic. Label by  $A_i$  the parabolic pairing the two faces above  $u_i$ . It follows that, for each  $i$ , the map  $A_i \cdots A_1$  sends  $v_{i+1}$  to  $v_1$  (see Figure 17). For each  $i > 1$ , there is a circle orthogonal to  $C$  that passes through  $u_i$  and  $u_{i+1}$ . Cut  $D$  along the dome above this circle, and translate the piece under this dome using  $A_i \cdots A_1$ . This procedure, analogous to that in Construction 3.4, rearranges pieces of  $D$  so that it only has a single vertex labelled  $\omega$ , at the expense of splitting all the vertices  $u_i$  into pairs. Since each  $A_i$  preserves the circle  $C$ , the images of the  $u_i$  still lie on the circle  $C$ .

after this cutting and gluing. In the running example, only one cut and glue need be done, along the dark dotted circle in [Figure 16\(D\)](#), to produce a polyhedron realising the cusp picture in [Figure 15\(B\)](#) (after doing the inversion across the dotted circle, the pattern of coloured vertices of [Figure 16\(D\)](#) becomes a subset of the dot pattern of [Figure 15\(B\)](#) but rotated by 90 degrees).

After this procedure has been done, we have produced a new right-angled ideal polyhedron, say  $D^*$ . Glue  $D^*$  to a copy  $\overline{D^*}$  of itself along the face supported on the dome above  $C$ . The result is a fundamental polyhedron  $D^* \cup \overline{D^*}$  for  $\mathbb{S}^3 \setminus \mathbf{l}$ , such that the lift of  $\omega$  is exactly one ideal vertex  $v$ . A concave lens can be constructed inside this polyhedron. Indeed, the geodesic plane formed by the dome above  $C$  contains  $v$  and the ideal vertices on the dome are only glued to other vertices on the dome by the side-pairing group; above each of these vertices there is an ideal octahedron, obtained by intersecting a horoball neighbourhood of each vertex on  $C$  with the faces of  $D^* \cup \overline{D^*}$  and coning the results to  $v$ .

That this concave lens satisfies the conditions (1)–(3) of [Theorem 4.2](#) follows from the observations earlier in the proof about the ideal vertices on  $C$ . Condition (4) is satisfied since all of the polyhedra are symmetric across the dome above  $C$  (since the whole fundamental domain is defined by such a reflection).  $\square$

**Example 4.6.** We consider the remaining planar cusps of [Figure 15](#). The cusp  $\dagger$ , [Figure 15\(C\)](#), does not satisfy the hypotheses of [Theorem 4.2](#) as both punctured discs it bounds are punctured by longitudes of other planar cusps. The cusp  $\ddagger$ , [Figure 15\(D\)](#), bounds exactly one punctured disc meeting the criteria and hence does satisfy the hypotheses of the theorem.

*Remark 4.7.* By adapting the argument used to prove [Theorem 4.5](#), one can show a dual result. Let  $\mathbf{l}$  be a fully augmented link  $\mathbf{l}$  with a planar cusp  $\omega_0$  such that:

- (i) There are no self-augmentations of  $\omega_0$ , and
- (ii) One of the two discs,  $D$ , bounded by  $\omega_0$  must be punctured only longitudinally by non-self-augmented planar cusps.

Then  $\omega_0$  forms the centre of a concave lens satisfying the conditions of [Theorem 4.2](#), and increasing the meridional length of  $\omega_0$  forms cone arcs in the geodesic surface  $D$  joining the augmentation cusp punctures together.

To prove this, consider the edge-coloured graph  $\Gamma$  as in the proof of [Theorem 4.5](#). Let  $\omega_1, \dots, \omega_k$  be the planar cusps puncturing  $D$ . The assumption (ii) implies that there is an edge-cycle in  $\Gamma$  for each  $i$  that is coloured alternately by  $\omega_i$  and by augmentation cusps. Take the dual circle pattern  $P$ ; there is a circle  $C_i$  in  $P$  for each  $\omega_i$ , as well as a circle  $C_0$  for the disc bounded by  $\omega_0$  that is *not*  $D$ . All these circles  $C_i$  for  $0 \leq i \leq k$  are tangent to a circle  $C$  corresponding to the disc  $D$ . Using products of side-pairing parabolics in each circle  $C_i$ , we may cut and glue all the  $\omega_i$ -tangency points on the circles onto the single  $\omega_i$ -point tangent to the circle  $C$  (i.e. we do the ‘glue by  $A_i \cdots A_1$ ’ step in the proof of [Theorem 4.5](#) for each circle  $C_i$ ). Since all of these side-pairings preserve the circle  $C_i$ , they do not introduce new vertices onto the circle  $C$  (it is only moving three vertices, and two of those get moved onto  $C_i$  away from the tangency point). Thus, after gluing, we obtain a fundamental polyhedron such that the face supported on the circle  $C$  meets ideal vertices corresponding to  $\omega_i$  for  $0 \leq i \leq k$ , and no other ideal vertices of polyhedron descend to  $\omega_i$ . This is enough to get a concave lens centred at  $\omega_0$  as described in the final paragraph of the proof of [Theorem 4.5](#).

**4.2. Further examples.** We end the paper with a final string of examples showing interesting phenomena that we do not have space to explore at length. In each case one can read off a relevant concave lens from the provided cusp picture, as in [Remark 4.3](#).

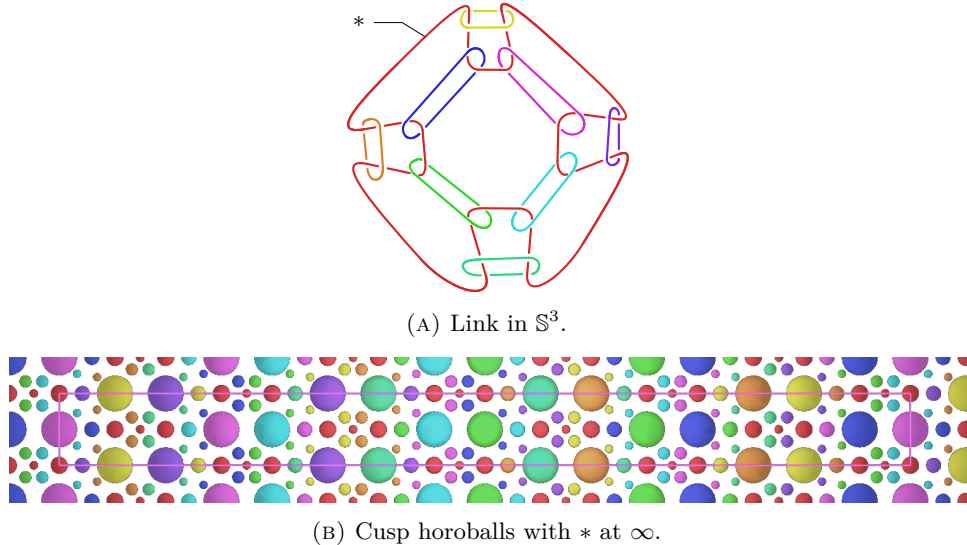
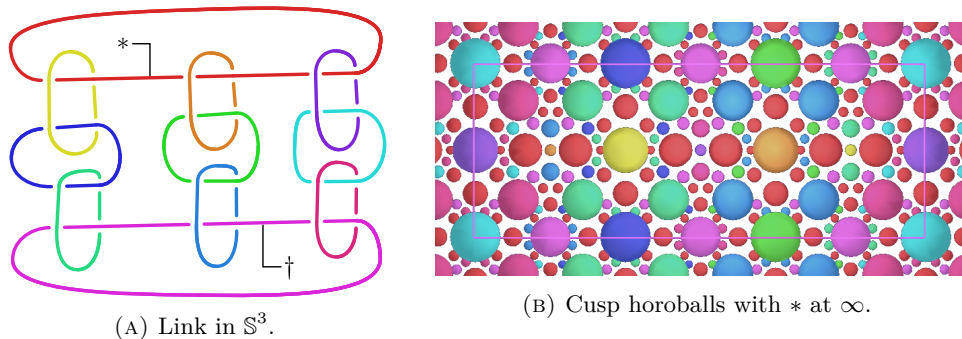
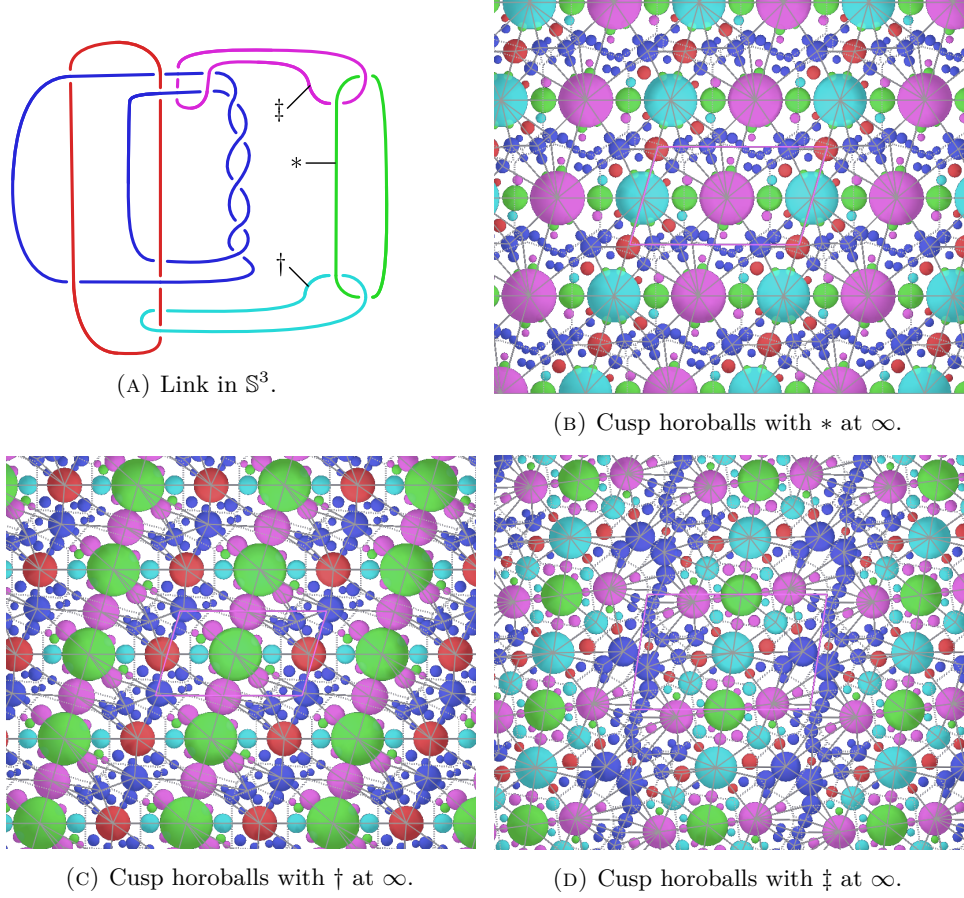
FIGURE 18. The Löbell link  $L(4)$ .

FIGURE 19. The augmented link from Example 4.9.

**Example 4.8.** This example will show that the non-self-augmentation condition of Theorem 4.5 cannot be removed. In Figure 18 we show the Löbell link  $L(4)$ , see Chesebro, DeBlois, and Wilton [12, §7.2]. Since the link is fully augmented, there is an embedded geodesic surface spanned by the long planar cusp  $*$ . However, it meets that cusp multiple times and as a consequence there are tetrahedra in the triangulation produced by the algorithm in the proof of Theorem 4.5 that contain two vertices descending to  $*$ ; it follows that there is no concave lens in this triangulation which has a central cusp corresponding to  $*$ . One can see in the horoball diagram there are vertices (in red) descending to  $*$ ; following the proof of Theorem 4.2, the vertex at infinity corresponding to  $*$  would remain parabolic while the other (equivalent) vertices would be pulled into ideal quadrilaterals, completely breaking the side-pairing combinatorics. In other words, no version of our cone deformations can be done along  $*$ .

**Example 4.9.** We now show a fully augmented link with two distinct cone-deformations centred at the same cusp. Consider the link of 11 components drawn in Figure 19(A).

FIGURE 20. A link obtained from [L11a202](#).

- The surface spanned by the cusp  $*$  which is punctured thrice by augmentation cusps is the centre of a concave lens satisfying the conditions of [Theorem 4.2](#). It can be deformed to produce six thrice-punctured spheres in total, two from each augmentation cusp. It is this lens which is centred in [Figure 19\(B\)](#).
- The other surface bounded by  $*$  in the reflection plane of the link is punctured by four longitudes and is the centre of a concave lens satisfying the conditions of [Remark 4.7](#); this lens is visible along the top and bottom horizontal edges of the rectangle in [Figure 19\(B\)](#). It can be deformed to obtain three new cone arcs so that, in the limit, the cusp  $\dagger$  splits into three thrice-punctured spheres.

**Example 4.10.** We consider now an example of a link with twist regions, to show that it is not enough for the cusp being elongated to be untwisted. In [Figure 20](#) we show a link obtained by adding a chain of three cusps to [L11a202](#). We can see cusp horoballs which give the outer vertices of a concave lens in [Figures 20\(B\)](#) and [20\(C\)](#) but not in [Figure 20\(D\)](#), even though all of the marked cusps bound embedded discs punctured only by meridians.

#### APPENDIX A. THE POLYHEDRON THEOREM FOR CONE MANIFOLDS

We describe here a generalisation for cone manifold groups of the Poincaré polyhedron theorem which can be proved by following the usual proof found, for

example, in Maskit [31, §IV.H]. It is certainly well-known to experts, and was used implicitly in Elzenaar [15]; its advantage in studying cone manifolds over the usual techniques via Thurston's gluing equations is that it gives an explicit presentation for the holonomy group. For further discussion on different polyhedron theorems see Epstein and Petronio [16].

Let  $\mathbb{X}$  be one of  $\mathbb{H}^n$ ,  $\mathbb{E}^n$ , or  $\mathbb{S}^n$  where  $n \geq 2$  and let  $\mathbb{G}$  be the isometry group of  $\mathbb{X}$ . Suppose that  $D \subset \mathbb{X}$  is an open polyhedron, i.e. a set that is locally an intersection of half-spaces in  $\mathbb{X}$ . Assume also that  $D$  has countably many faces, and is locally finite, i.e. the link of each vertex is a finite-sided polyhedron. For every facet  $s$  (codimension 1 face) of  $D$ , suppose that there is a facet  $s'$  of  $D$  (not necessarily distinct from  $s$ ) and an element  $g_s \in \mathbb{G}$  satisfying the following conditions:

- (i)  $g_s(s) = s'$ .
- (ii)  $g_{s'} = g_s^{-1}$ .
- (iii) There is an open neighbourhood  $U$  of  $s$  in  $D$  such that  $g_s(U) \cap U = \emptyset$ .

The side-pairing structure thus defined induces an equivalence relation on  $\overline{D}$  (in the case  $\mathbb{X} = \mathbb{H}^n$ ,  $\overline{D}$  also includes the boundary at infinity of  $D$ ) which is the identity on  $D$ . Let  $D^*$  be the quotient of  $\overline{D}$  by this relation with projection map  $p : \overline{D} \rightarrow D^*$ .

- (iv) For every  $z \in D^*$ ,  $p^{-1}(z)$  is a finite set.

A *generalised edge* of  $D$ , henceforth just *edge*, is either a codimension 2 face, or a point of tangency of two faces of  $D$  (meaningful only in the case  $\mathbb{X} = \mathbb{H}^n$ , where it behaves as an 'edge of length 0' with dihedral angle 0). For such an edge  $e$ , pick arbitrarily a facet  $s_1$  incident to  $e_1 = e$ . Then  $s'_1$  is adjacent to the translate  $g_{s_1}(e_1)$ . Now for each  $i$  let  $s_i$  be the facet incident to  $e_i$  that is distinct from  $s'_{i-1}$ . Let  $n = \min\{i \in \mathbb{N} : s_i = s_1 \text{ and } i > 1\}$ ; this minimum exists by (iv). The *edge cycle* of  $e$  is  $\{e_1, \dots, e_{n-1}\}$ . The *cycle transformation*  $h_e$  is by definition,  $g_{s_{n-1}} \cdots g_{s_1}$ . For each edge  $e$  of  $D$  let  $\alpha(e)$  be the dihedral angle of  $D$  across  $e$  and set

$$\theta(e) = \sum_{m=1}^n \alpha(e_m)$$

where  $\{e_1, \dots, e_n\}$  is the edge cycle of  $e$ .

- (v) The element  $h_e \in \mathbb{G}$  is a rotation through an angle  $\theta(e)$  if  $\theta(e) > 0$ . If  $\theta(e) = 0$  then necessarily  $\mathbb{X} = \mathbb{H}^n$ ; in this case  $h_e$  must be parabolic.

**Theorem A.1.** *Suppose that  $D \subset \mathbb{C}$  is a polyhedron with side-pairing maps  $(g_s)$  satisfying conditions (i)–(v) above. Let  $G = \langle g_s : s \text{ a side of } D \rangle$ . Then  $D^*$  admits a cone manifold structure locally modelled on  $\mathbb{X}$ , the singular locus of  $D^*$  is the projection of the set of edges  $e$  of  $D$  with  $\theta(e) \notin \{0, 2\pi\}$ , and  $G = \text{Hol}(D^*)$ . The relations induced by (ii) and (v) give a complete set of relations for  $G$ .*

*Proof.* One follows exactly the proof in Maskit [31, §IV.H], except we have replaced the condition on completeness with the parabolic cycle condition of (v). To see that the latter condition gives completeness of the path metric, note that the manifold is trivially complete everywhere except vertices on the sphere at infinity. It is here that we use that  $D$  is locally finite—if a sequence that is Cauchy in the hyperbolic metric is converging to such a point then it must eventually enter a horoball around it. We may assume the link of the polyhedron that is cut out by this horoball is finite, and the proof of Proposition IV.I.6 of Maskit [31] goes through.  $\square$

As mentioned in Elzenaar [15], versions of the Maskit combination theorems also go through for cone manifolds since they depend only on cutting and gluing fundamental domains and are just explicit versions of gluing results for general CAT(0) spaces: for instance, the first Maskit combination theorem is essentially found as Theorem II.11.18 of Bridson and Haefliger [7], and the second as Proposition II.11.21

*op. cit.* Both theorems just cited are global results on CAT(0) spaces. To recover the corresponding polyhedron theorems, one takes the fundamental polyhedra for the component groups being glued, produces a CAT(0) space from each by tiling with the side-pairings (one can view this as an infinitely branched cover of  $\mathbb{H}^3$ ), and then uses the global results on this tiled space—the proofs in [7] go by immediately slicing the space back up into fundamental polyhedra, gluing those together locally, and then developing the result to obtain a CAT(0) space on which the amalgamated group acts.

## REFERENCES

- [1] Colin Adams. “Unknotting tunnels in hyperbolic 3-manifolds”. In: *Math. Ann.* 302 (1995), pp. 177–195. DOI: [10.1007/BF01444492](https://doi.org/10.1007/BF01444492) (cit. on p. 14).
- [2] Colin C. Adams and Alan W. Reid. “Unknotting tunnels in two-bridge knot and link complements”. In: *Comment. Math. Helv.* 71 (1996), pp. 617–627. DOI: [10.1007/BF02566439](https://doi.org/10.1007/BF02566439) (cit. on p. 13).
- [3] Ian Agol. “Bounds on exceptional Dehn filling”. In: *Geom. Topol.* 4 (2000), pp. 431–449. DOI: [10.2140/gt.2000.4.431](https://doi.org/10.2140/gt.2000.4.431). arXiv: [math/9906183 \[math.GT\]](https://arxiv.org/abs/math/9906183) (cit. on p. 14).
- [4] Hirotaka Akiyoshi. “Thin representations for the one-cone torus group”. In: *Topology Appl.* 264 (2019), pp. 115–144. DOI: [10.1016/j.topol.2019.06.025](https://doi.org/10.1016/j.topol.2019.06.025) (cit. on p. 2).
- [5] Steven A. Bleiler and Craig D. Hodgson. “Spherical space forms and Dehn filling”. In: *Topology* 35 (1996), pp. 809–833. DOI: [10.1016/0040-9383\(95\)00040-2](https://doi.org/10.1016/0040-9383(95)00040-2) (cit. on p. 13).
- [6] Michel Boileau, Bernhard Leeb, and Joan Porti. “Geometrization of 3-dimensional orbifolds”. In: *Ann. of Math. (2)* 162 (2005), pp. 195–290. DOI: [10.4007/annals.2005.162.195](https://doi.org/10.4007/annals.2005.162.195). arXiv: [math/0010184 \[math.GT\]](https://arxiv.org/abs/math/0010184) (cit. on pp. 1, 14).
- [7] Martin R. Bridson and André Haefliger. *Metric spaces of non-positive curvature*. Grundlehren Math. Wiss. 319. Springer, 1999 (cit. on pp. 23, 24).
- [8] Jeffrey F. Brock and Kenneth W. Bromberg. “On the density of geometrically finite Kleinian groups”. In: *Acta. Math.* 192 (2004), pp. 33–93. DOI: [10.1007/BF02441085](https://doi.org/10.1007/BF02441085). arXiv: [math/0212189 \[math.GT\]](https://arxiv.org/abs/math/0212189) (cit. on p. 1).
- [9] K. Bromberg. “Hyperbolic cone-manifolds, short geodesics, and Schwarzian derivatives”. In: *J. Amer. Math. Soc.* 17 (2004), pp. 783–826. DOI: [10.1090/S0894-0347-04-00462-X](https://doi.org/10.1090/S0894-0347-04-00462-X). arXiv: [math/0211401 \[math.GT\]](https://arxiv.org/abs/math/0211401) (cit. on p. 1).
- [10] Danny Calegari. “A note on strong geometric isolation in 3-orbifolds”. In: *Bull. Aust. Math. Soc.* 53 (1996), pp. 271–280. DOI: [10.1017/S0004972700016993](https://doi.org/10.1017/S0004972700016993). arXiv: [math/0011126 \[math.GT\]](https://arxiv.org/abs/math/0011126) (cit. on p. 2).
- [11] Danny Calegari. “Napoleon in isolation”. In: *Proc. Amer. Math. Soc.* 129 (2001), pp. 3109–3119. DOI: [10.1090/S0002-9939-01-05915-9](https://doi.org/10.1090/S0002-9939-01-05915-9). arXiv: [math/9909106 \[math.GT\]](https://arxiv.org/abs/math/9909106) (cit. on p. 2).
- [12] Eric Chesebro, Jason DeBlois, and Henry Wilton. “Some virtually special hyperbolic 3-manifold groups”. In: *Comment. Math. Helv.* 87 (2012), pp. 727–787. DOI: [10.4171/CMH/267](https://doi.org/10.4171/CMH/267). arXiv: [0903.5288 \[math.GT\]](https://arxiv.org/abs/0903.5288) (cit. on p. 21).
- [13] Daryl Cooper, Jeffrey Danciger, and Anna Wienhard. “Limits of geometries”. In: *Trans. Amer. Math. Soc.* 370 (2018), pp. 6585–6627. DOI: [10.1090/tran/7174](https://doi.org/10.1090/tran/7174). arXiv: [1408.4109 \[math.GT\]](https://arxiv.org/abs/1408.4109) (cit. on p. 2).
- [14] Marc Culler, Nathan M. Dunfield, Matthias Goerner, and Jeffrey R. Weeks. *SnapPy, a computer program for studying the geometry and topology of 3-manifolds*. Version 3.2. URL: <http://snappy.computop.org> (cit. on pp. 3, 4).

- [15] Alex Elzenaar. *Changing topological type of compression bodies through cone manifolds*. 2024. arXiv: [2411.17940 \[math.GT\]](https://arxiv.org/abs/2411.17940) (cit. on pp. 2, 23).
- [16] David B. A. Epstein and Carlo Petronio. “An exposition of Poincaré’s polyhedron theorem”. In: *Enseign. Math. (2)* 40 (1994), pp. 113–170. DOI: [10.5169/seals-61108](https://doi.org/10.5169/seals-61108) (cit. on p. 23).
- [17] Benson Farb and Dan Margalit. *A primer on mapping class groups*. Princeton Math. Ser. Princeton University Press, 2012 (cit. on pp. 3, 13).
- [18] David Futer and Jessica S. Purcell. “Links with no exceptional surgeries”. In: *Comment. Math. Helv.* 82 (2007), pp. 629–664. DOI: [10.4171/CMH/105](https://doi.org/10.4171/CMH/105). arXiv: [math/0412307 \[math.GT\]](https://arxiv.org/abs/math/0412307) (cit. on pp. 11, 17).
- [19] David Futer, Jessica S. Purcell, and Saul Schleimer. “Effective bilipschitz bounds on drilling and filling”. In: *Geom. Topol.* 26 (2022), pp. 1077–1188. DOI: [10.2140/gt.2022.26.1077](https://doi.org/10.2140/gt.2022.26.1077). arXiv: [1907.13502 \[math.GT\]](https://arxiv.org/abs/1907.13502) (cit. on p. 1).
- [20] David Futer, Jessica S. Purcell, and Saul Schleimer. “Effective drilling and filling of tame hyperbolic 3-manifolds”. In: *Comment. Math. Helv.* 97 (2022), pp. 457–512. DOI: [10.4171/CMH/536](https://doi.org/10.4171/CMH/536). arXiv: [2104.09983 \[math.GT\]](https://arxiv.org/abs/2104.09983) (cit. on p. 1).
- [21] Sophie L. Ham and Jessica S. Purcell. “Geometric triangulations and highly twisted links”. In: *Alg. Geom. Topol.* 23 (2023), pp. 1399–1462. DOI: [10.2140/agt.2023.23.1399](https://doi.org/10.2140/agt.2023.23.1399). arXiv: [2005.11899 \[math.GT\]](https://arxiv.org/abs/2005.11899) (cit. on p. 17).
- [22] Michael Heusener, Joan Porti, and Eva Suárez. “Regenerating singular hyperbolic structures from Sol”. In: *J. Diff. Geom.* 59 (2001), pp. 439–478. DOI: [10.4310/jdg/1090349448](https://doi.org/10.4310/jdg/1090349448) (cit. on p. 2).
- [23] Craig D. Hodgson. “Degeneration and regeneration of geometric structures on three-manifolds”. Doctoral thesis. Princeton University, 1986 (cit. on p. 2).
- [24] Craig D. Hodgson and Steven P. Kerckhoff. “Rigidity of hyperbolic cone-manifolds and hyperbolic Dehn surgery”. In: *J. Diff. Geom.* 48 (1998), pp. 1–59. DOI: [10.4310/jdg/1214460606](https://doi.org/10.4310/jdg/1214460606) (cit. on pp. 2, 14).
- [25] Craig D. Hodgson and Steven P. Kerckhoff. “Universal bounds for hyperbolic Dehn surgery”. In: *Ann. of Math. (2)* 162 (2005), pp. 367–421. DOI: [10.4007/annals.2005.162.367](https://doi.org/10.4007/annals.2005.162.367) (cit. on p. 1).
- [26] Dionne Ibarra, Emma N. McQuire, and Jessica S. Purcell. *Augmented links, shadow links, and the TV volume conjecture: A geometric perspective*. 2025. arXiv: [2506.09296 \[math.GT\]](https://arxiv.org/abs/2506.09296) (cit. on pp. 3, 17).
- [27] Michael Kapovich. *Eisenstein series and Dehn surgery*. MSRI Preprint. 1992. URL: <https://www.math.ucdavis.edu/~kapovich/EPR/eis.pdf> (cit. on p. 2).
- [28] Sadayoshi Kojima. “Deformations of hyperbolic 3-cone-manifolds”. In: *J. Diff. Geom.* 49 (1998), pp. 469–516. DOI: [10.4310/jdg/1214461108](https://doi.org/10.4310/jdg/1214461108) (cit. on p. 2).
- [29] Marc Lackenby. “The volume of hyperbolic alternating link complements”. In: *Proc. London Math. Soc. (3)* 88 (2004). Appendix by Ian Agol and Dylan Thurston, pp. 204–224. DOI: [10.1112/S0024611503014291](https://doi.org/10.1112/S0024611503014291). arXiv: [math/0012185 \[math.GT\]](https://arxiv.org/abs/math/0012185) (cit. on p. 17).
- [30] Marc Lackenby. “Word hyperbolic Dehn surgery”. In: *Invent. Math.* 140 (2000), pp. 243–282. DOI: [10.1007/s002220000047](https://doi.org/10.1007/s002220000047). arXiv: [math/9808120 \[math.GT\]](https://arxiv.org/abs/math/9808120) (cit. on p. 14).
- [31] Bernard Maskit. *Kleinian groups*. Grundlehren Math. Wiss. 287. Springer-Verlag, 1987 (cit. on p. 23).
- [32] Grégoire Montcouquiol. “Deformations of hyperbolic convex polyhedra and cone-3-manifolds”. In: *Geom. Dedicata* 166 (2013), pp. 163–183. DOI: [10.1007/s10711-012-9790-5](https://doi.org/10.1007/s10711-012-9790-5) (cit. on p. 2).

- [33] Walter D. Neumann and Alan W. Reid. “Amalgamation and the invariant trace field of a Kleinian group”. In: *Math. Proc. Cambridge Philos. Soc.* 109 (1991), pp. 509–515. DOI: [10.1017/S0305004100069942](https://doi.org/10.1017/S0305004100069942) (cit. on p. 2).
- [34] Walter D. Neumann and Alan W. Reid. “Rigidity of cusps in deformations of hyperbolic 3-orbifolds”. In: *Math. Ann.* 295 (1993), pp. 223–237. DOI: [10.1007/BF01444885](https://doi.org/10.1007/BF01444885) (cit. on p. 2).
- [35] Grisha Perelman. *Ricci flow with surgery on three-manifolds*. 2003. arXiv: [math/0303109 \[math.DG\]](https://arxiv.org/abs/math/0303109) (cit. on p. 14).
- [36] Grisha Perelman. *The entropy formula for the Ricci flow and its geometric applications*. 2002. arXiv: [math/0211159 \[math.DG\]](https://arxiv.org/abs/math/0211159) (cit. on p. 14).
- [37] Tali Pinsky, Jessica S. Purcell, and José Andrés Rodríguez-Migueles. “Arithmetic modular links”. In: *Pacific J. Math.* 327 (2023), pp. 337–358. DOI: [10.2140/pjm.2023.327.337](https://doi.org/10.2140/pjm.2023.327.337). arXiv: [2307.09409 \[math.GT\]](https://arxiv.org/abs/2307.09409) (cit. on pp. 3, 11).
- [38] Joan Porti. “Regenerating hyperbolic and spherical cone structures from Euclidean ones”. In: *Topology* 37 (1998), pp. 365–392. DOI: [10.1016/S0040-9383\(97\)00025-6](https://doi.org/10.1016/S0040-9383(97)00025-6) (cit. on p. 2).
- [39] Joan Porti. “Regenerating hyperbolic cone structures from Nil”. In: *Geom. Topol.* 6 (2002), pp. 815–852. DOI: [10.2140/gt.2002.6.815](https://doi.org/10.2140/gt.2002.6.815). arXiv: [math/0212298 \[math.GT\]](https://arxiv.org/abs/math/0212298) (cit. on p. 2).
- [40] Jessica S. Purcell. “An introduction to fully augmented links”. In: *Interactions between hyperbolic geometry, quantum topology and number theory. Proceedings of a workshop, June 3–13, 2009 and a conference, June 15–19, 2009, Columbia University, New York, NY, USA*. Ed. by Abhijit Champanerkar, Oliver Dasbach, Efstratia Kalfagianni, Ilya Kofman, Walter Neumann, and Neal Stoltzfus. *Contemp. Math.* 541. 2011, pp. 205–220 (cit. on pp. 3, 17, 19).
- [41] Jessica S. Purcell. “Cusp shapes under cone deformation”. In: *J. Diff. Geom.* 80 (2008), pp. 453–500. DOI: [10.4310/jdg/1226090484](https://doi.org/10.4310/jdg/1226090484). arXiv: [math/0410233 \[math.GT\]](https://arxiv.org/abs/math/0410233) (cit. on p. 2).
- [42] William P. Thurston. “How to see 3-manifolds”. In: *Classical Quantum Gravity* 15 (1998), pp. 2545–2571. DOI: [10.1088/0264-9381/15/9/004](https://doi.org/10.1088/0264-9381/15/9/004) (cit. on pp. 1, 3).
- [43] William P. Thurston. *The geometry and topology of three-manifolds*. Ed. by Steven P. Kerckhoff. Vol. IV of collected works; originally published c.1979. American Mathematical Society, 2022 (cit. on pp. 1, 3, 11).
- [44] Hartmut Weiß. “Global rigidity of 3-dimensional cone-manifolds”. In: *J. Diff. Geom.* 76 (2007), pp. 495–523. DOI: [10.4310/jdg/1180135696](https://doi.org/10.4310/jdg/1180135696) (cit. on p. 2).
- [45] Hartmut Weiß. “Local rigidity of 3-dimensional cone-manifolds”. In: *J. Diff. Geom.* 71 (2005), pp. 437–506. DOI: [10.4310/jdg/1143571990](https://doi.org/10.4310/jdg/1143571990) (cit. on p. 2).
- [46] Hartmut Weiß. “The deformation theory of hyperbolic cone-3-manifolds with cone-angles less than  $2\pi$ ”. In: *Geom. Topol.* 17 (2013), pp. 329–367. DOI: [10.2140/gt.2013.17.329](https://doi.org/10.2140/gt.2013.17.329) (cit. on p. 2).
- [47] Norbert Wielenberg. “The structure of certain subgroups of the Picard group”. In: *Math. Proc. Cambridge Philos. Soc.* 84 (1978), pp. 427–436. DOI: [10.1017/s0305004100055250](https://doi.org/10.1017/s0305004100055250) (cit. on pp. 3, 6).
- [48] Ken’ichi Yoshida. “Degeneration of 3-dimensional hyperbolic cone structures with decreasing cone angles”. In: *Conform. Geom. Dyn.* 26 (2022), pp. 182–193. DOI: [10.1090/ecgd/375](https://doi.org/10.1090/ecgd/375). arXiv: [1909.06622 \[math.GT\]](https://arxiv.org/abs/1909.06622) (cit. on p. 2).